Chapter 5

Doping dependence of chemical potential in $Nd_{1-x}Sr_xMnO_3$

Part of this chapter has been published in

- "Photoemission Study of Perovskite-type Manganites with Stripe Ordering" by K. Ebata, H. Wadati, M. Takizawa, K. Maekawa, A. Fujimori, A. Chikamatsu, H. Kumigashira, M. Oshima, Y. Tomioka, H. Kuwahara, and Y. Tokura, J. Supercond. Nov. Magn. **20**, 543-546 (2007).

5.1 Introduction

Systems with intermediate and small band width such as $Nd_{1-x}Sr_xMnO_3$ (NSMO) and $Pr_{1-x}Ca_xMnO_3$ (PCMO) exhibit the so-called CE-type antiferromagnetic (AF) charge-ordered (CO) phase in the doping region around the half-doping $x = 0.5$ as shown in the phase diagram of Fig. 5.1 [5.1, 2, 3]. A stripe formation has been found in the CO phase of $La_{1-x}Ca_xMnO_3$ or PCMO [5.4, 5, 6, 7]. The periodicity of the stripes in $La_{1-x}Ca_xMnO_3$ or PCMO changes gradually with hole doping and temperature [5.4, 5, 6, 7].

The carrier concentration dependence of the chemical potential provides deep insight into the electronic structure of materials. In Chapter 3, we have described the suppression of the chemical potential shift ($\Delta\mu$) as a function of carrier concentration due to incommensurate charge modulation in PCMO [5.8]. Also, a pinning of the $\Delta\mu$ due to static or dynamic stripe formation was observed for $La_{2-x}Sr_xCuO_4$ and $La_{2-x}Sr_xNiO_4$ [5.9, 10]. The suppression of $\Delta\mu$ occurs when the periodicity of stripes changes with hole doping. On the other hand, the $\Delta\mu$ in $La_{1-x}Sr_xMnO_3$ (LSMO), which has the widest bandwidth among the manganites, exhibited a monotonous shift without indication of chemical potential pinning [5.11, 12]. PCMO thin films grown

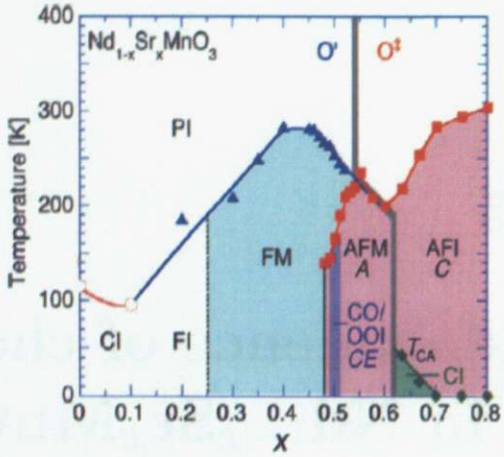

Figure 5.1: Electronic phase diagram of $Nd_{1-x}Sr_xMnO_3$. PI: Paramagnetic insulating phase; CI: Spin-canted insulating phase; FM: Ferromagnetic metallic phase; FI: Ferromagnetic insulating phase; CO/OOI: Charge-orbital ordered insulating phase; AFM: Antiferromagnetic metallic phase; AFI: Antiferromagnetic insulating phase [5.1, 3].

on $LaAlO_3$ (001) substrates, which show the suppression of the CO phase due to a compressive strain, exhibits a monotonous chemical potential shift at least up to $x = 0.5$, too [5.13, 14, 15]. It is therefore considered that there is no intrinsic stripe formation in the strained PCMO films with the suppressed CO phase as well as in LSMO.

In this chapter, we have measured the doping-dependent chemical potential shift of the intermediate-bandwidth system NSMO by core-level photoemission spectroscopy. A suppression of the $\Delta\mu$ was observed near and in the CE-type CO composition range of NSMO, related to the incommensurate charge modulation.

5.2 Experimental

Single crystals of NSMO ($x = 0.4$, 0.45, 0.5, 0.55, 0.6, and 0.7) were prepared by the floating zone method [5.1]. These samples were supplied by Prof. H. Kuwahara of Sophia University and Dr. Y. Tomioka and Prof. Y. Tokura of National Institute of Advanced Industrial Science and Technology. X-ray photoemission measurements were performed using a Mg $K\alpha$ source ($h\nu = 1253.6$ eV) and a SCIENTA SES-100 analyzer. The energy resolution including the x-ray source and the analyzer was about 800 meV

but we could determine the shifts of the core levels to an accuracy of ± 40 meV when the spectral line shape was almost independent of chemical composition as in the previous studies of chemical potential shift [5.8, 16]. The measured binding energies were stable, judged from the fact that the gold $4f_{7/2}$ core-level spectrum was nearly unchanged throughout the measurements. All the photoemission measurements were performed under the base pressure of $\sim 10^{-10}$ Torr at room temperature. The sample surfaces were repeatedly scraped *in situ* with a diamond file to obtain clean surfaces. The cleanliness of the surfaces was checked by the weakness of contamination- or degradation-related feature on the higher binding energy side of the O 1s peak.

5.3 Results and discussion

Figure 5.2 shows the spectra of the O 1s, Sr 3d, Nd 3d and Mn 2p core levels. The vertical lines mark the estimated positions of the core levels employed in the present study. For the O 1s core level, we have used the midpoint of the low binding-energy slope because the line shape on the higher binding energy side of the O 1s spectra is known to be sensitive to surface contamination or degradation. We have also used the midpoint for the Sr 3d core level for the same reason. The shifts of the Nd 3d and Mn 2p core levels have been determined from their peak position because the line shapes of the Nd 3d and Mn 2p core levels slightly changed with composition and the midpoint position depended on the peak width.

In Fig. 5.3(a), we have plotted the binding energy shift ΔE_B of each core level as a function of hole concentration. One can see that the O 1s, Sr 3d and Nd 3d core levels are shifted in the same direction, while the Mn 2p core level moves in the opposite direction. The opposite shift of the Mn 2p core level can be ascribed to the change of the Mn valence with hole doping [5.8]. Therefore, we conclude that the nearly same shifts of the O 1s, Sr 3d and Nd 3d core levels reflect the $\Delta\mu$, and take the average of the shifts of the three core levels as a measure of $\Delta\mu$ in NSMO [5.8].

In Fig. 5.3(b), we have plotted the $\Delta\mu$ of NSMO as a function of carrier concentration thus deduced. A clear downward chemical potential shift with hole concentration is observed in the regions $x \lesssim 0.45$ and $x \gtrsim 0.55$, as reported for LSMO [5.11]. However, a weak suppression of the shift is observed in and near the CE-type CO composition range $0.45 \lesssim x \lesssim 0.55$, corresponding to the narrow region of the CO phase in the phase diagram of NSMO as shown in Fig. 5.1 [5.1, 3]. The PCMO shows a strong suppression of the $\Delta\mu$ in and near the CE-type CO composition range as shown in

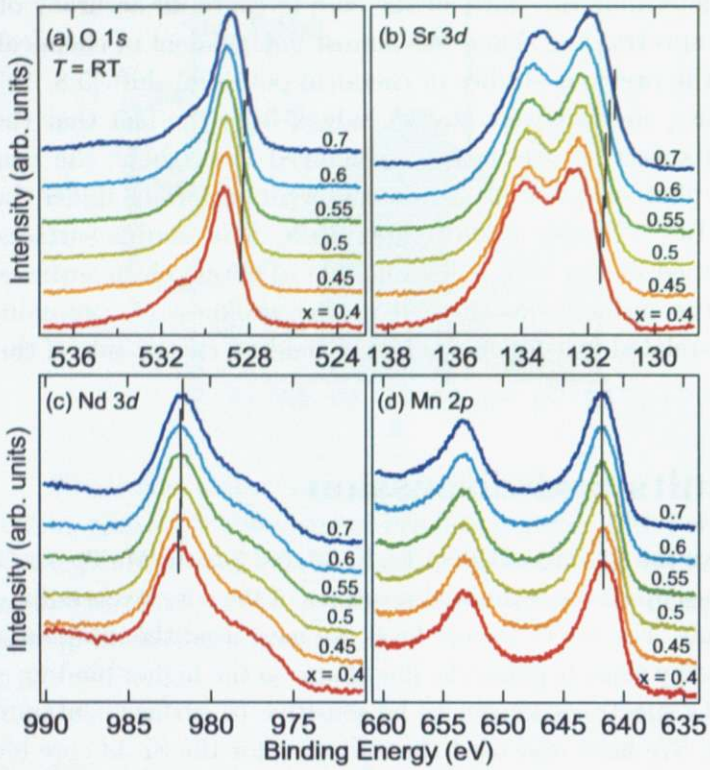

Figure 5.2: Core-level photoemission spectra of $Nd_{1-x}Sr_xMnO_3$ taken with the Mg $K\alpha$ line. (a) O 1s; (b) Sr 3d; (c) Nd 3d; (d) Mn 2p. The intensity has been normalized to the peak height.

Chapter 3 [5.8]. Such a chemical potential pinning was not observed in bulk and thin film LSMO in which the CO phase was not found. PCMO thin films grown on $LaAlO_3$ substrates, where the CO phase was suppressed by compressive strain from the substrates, did not exhibited the pinning of chemical potential up to $x = 0.5$, too [5.14, 15, 11, 12]. If the suppression is due to an electronic phase separation as the thermodynamic relationship suggests, the phase separation can occur only on a microscopic scale as in the bi-stripe or Wigner-crystal model suggested for $La_{1-x}Ca_xMnO_3$ for $x \geq 0.5$ [5.4, 5] because the accumulation of long-range Coulomb energy has to be avoided. Although our measurements were performed for the PI phase above the CO transition temperature in NSMO, the fluctuations of CO state in NSMO observed in the PI phase by means of x-ray scattering studies [5.17] seems to be sufficient to suppress the $\Delta\mu$. Therefore, we attribute the suppression of the $\Delta\mu$ to a charge self-organization such as the stripe

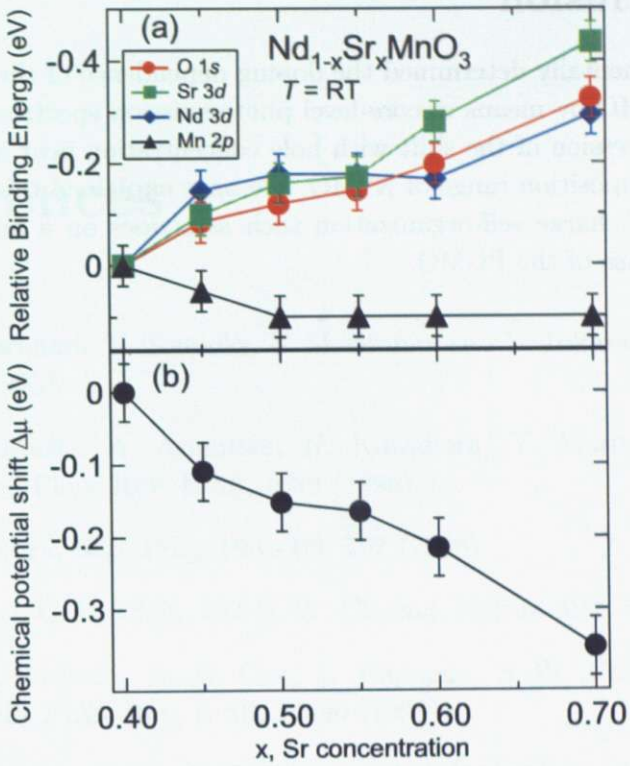

Figure 5.3: Core-level shifts and chemical potential shift. (a) Binding energy shifts of the O 1s, Sr 3d, Nd 3d, and Mn 2p core levels as functions of carrier concentration x; (b) Chemical potential shift $\Delta\mu$ in $Nd_{1-x}Sr_xMnO_3$ as a function of carrier concentration x.

formation on a microscopic scale. For the CE-type CO composition range of NSMO and PCMO, it is considered that the rigid-band picture breaks down as in the case of high-T_c cuprates in the underdoped region, where the pseudogap is opened [5.8, 9, 18].

Since the Monte Carlo simulation on a one-orbital model has suggested that the effect of disorder has influence on the $\Delta\mu$, disorder strength in NSMO has to be evaluated [5.19]. According to the variance of the ionic radii of the A-site cations, the effect of disorder in NSMO as well as that in PCMO and LSMO is relatively small [5.20]. The suppression of $\Delta\mu$ in NSMO and PCMO is therefore consistent with the weakness of disorder effect [5.20].

5.4 Conclusion

We have experimentally determined the doping dependence of the chemical potential in NSMO by means of core-level photoemission spectroscopy. We observed a suppression of the shift with hole concentration near and in the CE-type CO composition range of NSMO. We have explained this suppression as due to a charge self-organization such as stripes on a microscopic scale as in the case of the PCMO.

References

[5.1] H. Kuwahara, Y. Tomioka, Y. Moritomo, and Y. Tokura, Science **270**, 961 (1995).

[5.2] Y. Tomioka, A. Asamitsu, H. Kuwahara, Y. Moritomo, and Y. Tokura, Phys. Rev. B **53**, 1689 (1996).

[5.3] Y. Tokura, Rep. Prog. Phys **69**, 797 (2006).

[5.4] S. Mori, C. H. Chen, and S.-W. Cheong, Nature **392**, 473 (1998).

[5.5] P. G. Radaelli, D. E. Cox, L. Capogna, S.-W. Cheong, and M. Marezio, Phys. Rev. B **59**, 14440 (1999).

[5.6] G. C. Milward, M. J. Calderon, and P. B. Littlewood, Nature **433**, 607 (2005).

[5.7] C. H. Chen, S. Mori, and S.-W. Cheong, Phys. Rev. Lett. **83**, 4792 (1999).

[5.8] K. Ebata, H. Wadati, M. Takizawa, A. Fujimori, A. Chikamatsu, H. Kumigashira, M. Oshima, Y. Tomioka, and Y. Tokura, Phys. Rev. B **74**, 064419 (2006).

[5.9] A. Ino, T. Mizokawa, A. Fujimori, K. Tamasaku, H. Eisaki, S. Uchida, T. Kimura, T. Sasagawa, and K. Kishio, Phys. Rev. Lett. **79**, 2101 (1997).

[5.10] M. Satake, K. Kobayashi, T. Mizokawa, A. Fujimori, T. Tanabe, T. Katsufuji, and Y. Tokura, Phys. Rev. B **61**, 15515 (2000).

[5.11] J. Matsuno, A. Fujimori, Y. Takeda, and M. Takano, Europhys. Lett. **59**, 252 (2002).

[5.12] K. Horiba, A. Chikamatsu, H. Kumigashira, M. Oshima, N. Nakagawa, M. Lippmaa, K. Ono, M. Kawasaki, and H. Koinuma, Phys. Rev. B **71**, 155420 (2005).

[5.13] H. Wadati, A. Maniwa, A. Chikamatsu, I. Ohkubo, H. Kumigashira, M. Oshima, A. Fujimori, M. Lippmaa, M. Kawasaki, and H. Koinuma, Phys. Rev. Lett. in press

[5.14] H. Wadati, A. Maniwa, I. Ohkubo, H. Kumigashira, A. Fujimori, M. Oshima, M. Lippmaa, M. Kawasaki, and H. Koinuma, J. Magn. Magn. Mater **310**, 963 (2007).

[5.15] Z. Q. Yang, Y. Q. Zhang, J. Aarts, M.-Y. Wu, and H. W. Zandbergen, Appl. Phys. Lett. **88**, 072507 (2006).

[5.16] H. Yagi, T. Yoshida, A. Fujimori, Y. Kohsaka, M. Misawa, T. Sasagawa, H. Takagi, M. Azuma, and M. Takano, Phys. Rev. B **73**, 172503 (2006).

[5.17] V. Kiryukhin, T. Y. Koo, A. Borissov, Y. J. Kim, C. S. Nelson, J. P. Hill, D. Gibbs, and S.-W. Cheong, Phys. Rev. B **65**, 094421 (2002).

[5.18] N. Harima, A. Fujimori, T. Sugaya, and I. Terasaki, Phys. Rev. B **67**, 172501 (2003).

[5.19] A. Moreo, M. Mayr, A. Feiguin, S. Yunoki, and E. Dagotto, Phys. Rev. Lett. **84**, 5568 (2000).

[5.20] Y. Tomioka and Y. Tokura, Phys. Rev. B **70**, 014432 (2004).

Chapter 6

Temperature dependence of chemical potential in $Nd_{1-x}Sr_xMnO_3$

Part of this chapter has been published in

- "Photoemission Study of Perovskite-type Manganites with Stripe Ordering" by K. Ebata, H. Wadati, M. Takizawa, K. Maekawa, A. Fujimori, A. Chikamatsu, H. Kumigashira, M. Oshima, Y. Tomioka, H. Kuwahara, and Y. Tokura, J. Supercond. Nov. Magn. **20**, 543-546 (2007).

6.1 Introduction

Historically, the magnetic and transport properties of manganites have been understood in terms of double-exchange (DE) interaction between the localized t_{2g} electrons and the itinerant e_g electrons [6.1, 2, 3]. In this model, the kinetic energy gain of the holes doped into the e_g band is maximized when the spins of the t_{2g} electrons are aligned in the same direction, thereby stabilizing the ferromagnetic ground state. However, it has been pointed out by Millis *et al.* [6.4] that the DE model is insufficient to explain the huge change in the resistivity under a magnetic field and the high resistivity above the Curie temperature (T_C). They have proposed a model including the dynamical Jahn-Teller (JT) distortion of the MnO_6 octahedra in addition to the DE interaction and reproduced the experimentally observed behavior of the resistivity. It has also been proposed that the extraordinary enhancement of the resistivity in the manganites may result from the emergence of lattice polarons in the paramagnetic insulating (PI) phase [6.4, 5, 6, 7]. Koo *et al.*

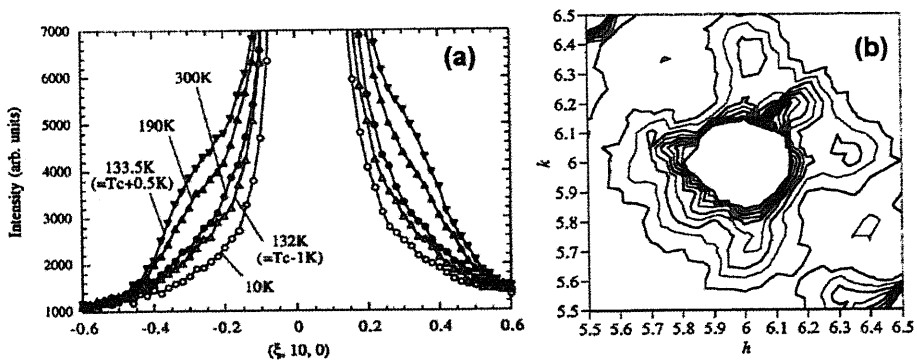

Figure 6.1: X-ray scattering results for $(Nd_{0.125}Sm_{0.875})_{0.52}Sr_{0.48}MnO_3$ (T_C = 133 K) [6.5]. (a) Temperature dependence of the scattering intensity in the vicinity of one Bragg point due to diffuse scattering. (b) Butterfly-shaped pattern of the diffuse scattering around the Bragg peak.

[6.8] have found that lattice polarons in $Nd_{0.7}Sr_{0.3}MnO_3$ are strongly suppressed by applying magnetic field and do not completely disappear at high fields, corresponding to an admixture of the "conducting" and "insulating" carriers. From x-ray scattering and neutron scattering studies [6.5, 6, 7], indeed, the diffuse scattering due to the lattice polarons has been observed in the high-temperature PI phase of manganites and gradually disappears with decreasing temperature in the ferromagnetic metallic (FM) phase as shown in Fig. 6.1. On the other hand, several local structural studies have suggested that a dynamical or local JT distortion persists in the FM phase, too. X-ray absorption fine structure (EXAFS) studies have shown that the lattice distortion of the MnO_6 octahedra is found in the FM phase of $La_{1-x}Ca_xMnO_3$ at low temperatures [6.9, 10]. From the pair-density function analysis of pulsed neutron diffraction data, the local JT distortion has been observed in the FM phase of $La_{1-x}Sr_xMnO_3$ [6.11]. If the JT distortion exists in the FM phase, the degeneracy of the e_g band may be lifted already in that phase.

In order to obtain insight into the competition between the DE mechanism and the lattice-polaron effect, the measurement of chemical potential shift ($\Delta\mu$) as a function of temperature gives much insight. According to the DE model, temperature-dependent chemical potential shift occurs due to the change in the e_g bandwidth as schematically shown in Fig. 6.2 [6.12]. If the e_g band is split by JT distortion and the one-orbital DE model becomes relevant, the chemical potential is shifted upward for hole concentration x<0.5 with decreasing temperature and downward for x>0.5 [6.12]. If one takes

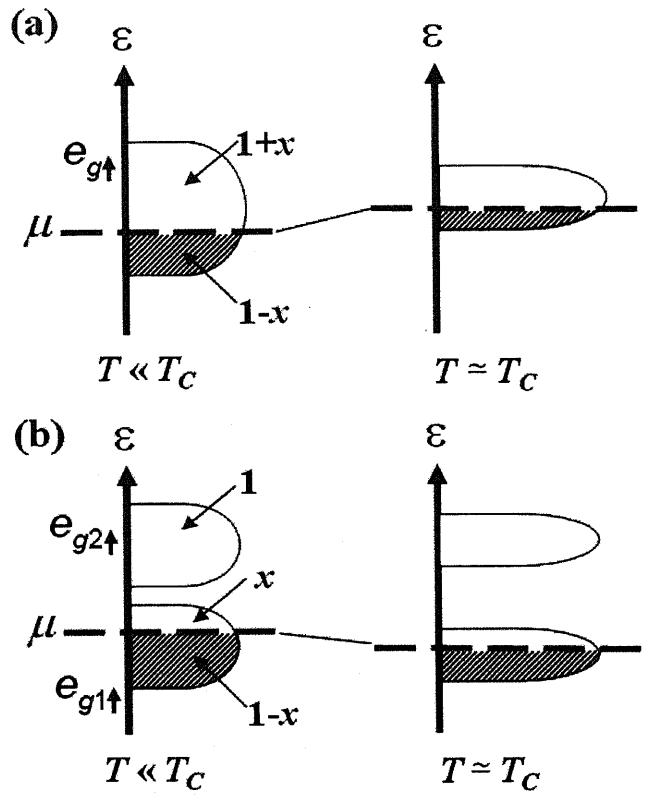

Figure 6.2: Schematic pictures of the temperature-dependent DOS due to the DE interaction in FM phase for x<0.5. (a) Degenerate two-orbital model; (b) One-orbital model resulting from the Jahn-Teller splitting. μ, T_C and x denote the chemical potential, the Curie temperature and the hole concentration, respectively.

into account the double degeneracy of the e_g orbitals [Fig. 6.2(a)], a downward shift with decreasing temperature would be expected in the FM phase for 0<x<1 because the up-spin band of the e_g orbitals is less than half-filled in the $R_{1-x}A_xMnO_3$ compounds. Therefore, the temperature-dependent chemical potential shift is sensitive to the splitting of the e_g band and therefore to the dynamical/local JT effect. Schulte *et al.* [6.13] have investigated the change of the work function in $La_{1.2}Sr_{1.8}Mn_2O_7$ as a function of temperature by measurements of photoemission spectra and attributed the change to the temperature-dependent shift of chemical potential. Alternatively, the chemical potential shift can be deduced from the shifts of photoemission spectra because the binding energies of the spectra are measured relative to

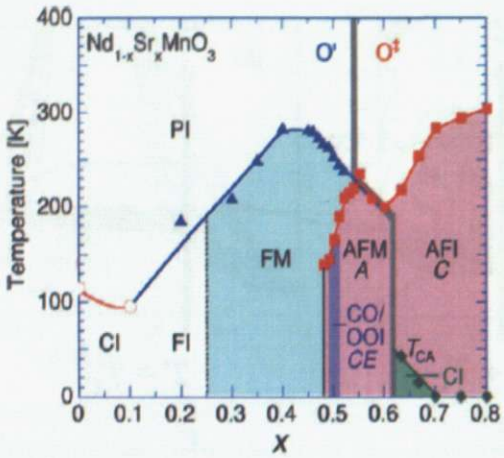

Figure 6.3: Electronic phase diagram of $Nd_{1-x}Sr_xMnO_3$. PI: Paramagnetic insulating phase; CI: Spin-canted insulating phase; FM: Ferromagnetic metallic phase; FI: Ferromagnetic insulating phase; CO/OOI: Charge-orbital ordered insulating phase; AFM: Antiferromagnetic metallic phase; AFI: Antiferromagnetic insulating phase [6.14, 15].

the chemical potential. We employ the latter method in this work.

$Nd_{1-x}Sr_xMnO_3$ (NSMO) is a suitable system for clarifying the relationship between the DE interactions and the existence of lattice polarons because it shows the FM phase for $x \lesssim 0.5$ and the so-called CE-type antiferromagnetic (AF) charge-ordered (CO) phase in the doping region close to the half-doping $x = 0.5$ as shown in Fig. 6.3 [6.14, 15]. In this work, we study the chemical potential shift in NSMO as a function of temperature by measurements of core-level photoemission spectra. We found that the chemical potential shift was large in the low-temperature part of the FM phase as predicted by the DE model and dynamical/local JT effect and was suppressed at high temperatures near T_C. We consider that the different behaviors with temperature to be related to the competition between the DE interaction and the lattice-polaron effect. We also observed the temperature-dependent chemical potential shifts in the CE-type AF charge-ordered ($x = 0.5$), A-type AF metallic ($x = 0.55$ and 0.6), and C-type AF insulating ($x = 0.7$) phases of NSMO.

6.2 Experimental

Single crystals of NSMO ($x = 0.4$, 0.45, 0.5, 0.55, 0.6, and 0.7) were prepared by the floating zone method [6.14]. These samples were supplied by Prof. H. Kuwahara of Sophia University and Dr. Y. Tomioka and Prof. Y. Tokura of National Institute of Advanced Industrial Science and Technology. X-ray photoemission spectroscopy measurements were performed using the photon energies of $h\nu = 1253.6$ eV (Mg $K\alpha$). All the photoemission measurements were performed under the base pressure of $\sim 10^{-10}$ Torr at 20-330 K. The samples were repeatedly scraped *in situ* with a diamond file to obtain clean surfaces. The cleanliness of the sample surface was checked by the reduction of the shoulder on the high binding energy side of the O 1s core level. Photoelectrons were collected using a Scienta SES-100 electron-energy analyzer. The energy resolution was about 800 meV. The measured binding energies were stable, because the gold $4f_{7/2}$ core-level spectrum did not changed in the measurements with the accuracy of ± 10 meV at each temperature.

6.3 Results and discussion

In Fig. 6.4, we have plotted the spectra of the O 1s, Sr 3d, Nd 3d and Mn 2p core levels in NSMO with $x = 0.4$. The vertical lines mark the estimated positions of the core levels used in the present study. We employed the midpoint of the low binding-energy slope for the O 1s core level because the line shape on the higher-binding energy side of the O 1s spectra is known to be affected by surface contamination or degradation. We also employed the midpoint for the Sr 3d and Mn 2p core levels. As for the Nd 3d core level, 80 % of the peak height of the low binding-energy slope was used because the line shape near the midpoint on the lower-binding energy side slightly changed with temperature.

Recently hard x-ray photoemission spectroscopy has revealed that a well-screened feature is observed on the low binding-energy side of Mn $2p_{3/2}$ main peak in the FM phase of $La_{1-x}Sr_xMnO_3$ thin films [6.16, 17]. The well-screened peak is known to originate from core-hole screening through the evolution of density of states at the Fermi level [6.16, 17]. This peak was not clearly observed in our measurements due to lower energy resolution and partly due to the short mean free paths of the emitted low kinetic energy electrons. However, because the doping-dependent shifts of the Mn 2p and O 1s core levels of the $La_{1-x}Sr_xMnO_3$ observed by hard x-ray measurements are in good agreement with that in soft x-ray measurements owing to the low intensity of the well-screened peak [6.16, 17, 18, 19], we consider that the well-screened peak does not influence on the estimation of core-level shifts.

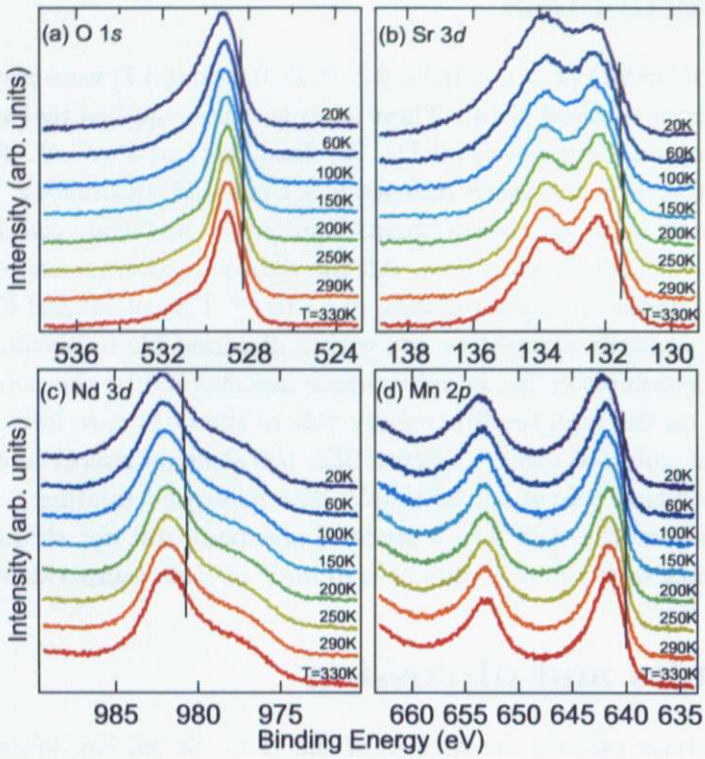

Figure 6.4: Core-level photoemission spectra of $Nd_{0.6}Sr_{0.4}MnO_3$ taken with the Mg $K\alpha$ line. (a) O 1s; (b) Sr 3d; (c) Nd 3d; (d) Mn 2p.

Figure 6.5(a) shows the binding energy shift of each core level as a function of temperature for NSMO with $x = 0.4$. One can see that the observed binding energy shifts with temperature were approximately common to the O 1s, Sr 3d, Nd 3d and Mn 2p core levels. In the measurements of the doping-dependent chemical potential shift in $Pr_{1-x}Ca_xMnO_3$, all the core levels have shown identical shifts with hole concentration except for the Mn 2p core level, where the effect of chemical shift is superimposed [6.20]. Here, all the core levels including the Mn 2p core level exhibit similar shifts with temperature in contrast to the measurements of doping-dependent core-level shifts [6.20]. Therefore, we assume that the shifts of the core levels are largely due to the chemical potential shift, and take the average of the shifts of the four core levels as a measure of $\Delta\mu$ as a function of temperature in NSMO.

Figure 6.5(b) shows the temperature-dependent chemical potential shift in NSMO with $x = 0.4$. We observed a large upward chemical potential shift with decreasing temperature in the FM phase of NSMO at low temperatures.

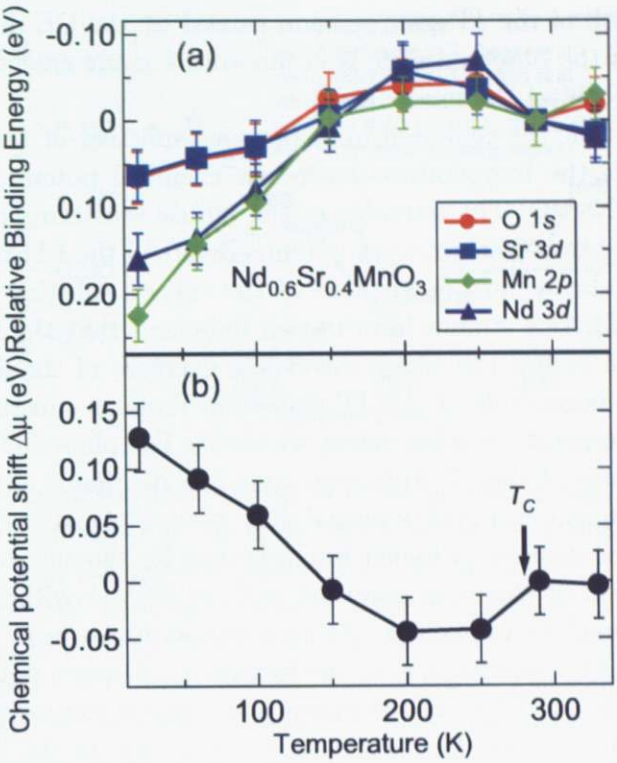

Figure 6.5: Core-level shifts and chemical potential shift in $Nd_{0.6}Sr_{0.4}MnO_3$. (a) Binding energy shifts of the O $1s$, Sr $3d$, Nd $3d$, and Mn $2p$ core levels as functions of temperature relative to 290 K; (b) Chemical potential shift $\Delta\mu$ as a function of temperature. T_C denotes Curie temperature.

Furukawa [6.12] proposed an anomalous temperature-dependent chemical potential shift below T_C due to the DE interaction through the change of the e_g bandwidth with temperature. He also predicted that the magnitude of the shift was estimated to be about 0.1 eV when the e_g bandwidth was of order $\sim$ 1 eV [6.12]. If the e_g band remains degenerate in the FM phase of NSMO, one would expect to see a downward chemical potential shift with decreasing temperature based on the DE interaction because the up-spin band of the e_g orbitals is less than half-filled for $0<x<1$. On the other hand, if the degeneracy of the e_g band is lifted by the dynamical/local JT distortion, the upward chemical potential shift with decreasing temperature is predicted because the band is more than half filled for $x<0.5$ (see Fig. 6.2). Therefore, we attribute the large upward shift of the chemical potential with decreasing temperature in the low-temperature FM phase of NSMO to the

change in the width of the JT-split e_g band caused by the DE mechanism. The magnitude of the observed shift is in quantitative agreement with the results of the one-orbital DE model [6.12].

We consider that the temperature-dependent splitting of the e_g band may also influence the temperature-dependent chemical potential shift in the FM phase of NSMO. The intensity of the diffuse scattering due to JT effect gradually increases with increasing temperature in the FM phase near T_C, which may indicate further increase of the energy splitting of the e_g level [6.5, 6, 7]. EXAFS studies have indeed indicated that the transition from the PI phase to the FM phase involves a decrease of the JT distortion but that the magnitude of the JT distortion remains substantial and becomes nearly temperature-independent within the FM phase [6.9]. If temperature dependence of the JT distortion were the dominant cause of the temperature-dependent chemical potential shift, the temperature-dependent shift would be even stronger at higher temperatures for the one-orbital case and the suppression of chemical potential shift in NSMO within the FM phase near T_C cannot be explained. At high temperatures near T_C in the PI phase, the diffuse scattering due to the formation of lattice polarons has been observed by means of x-ray scattering and neutron scattering studies [6.5, 6, 7]. We consider that the suppression of the shift in the FM phase at high temperatures is connected with the influence of the lattice polarons and the DE model is no more effective at those high temperatures.

In Fig. 6.6, we compare $\Delta\mu$ for NSMO ($x = 0.4$) with the shifts of the O 1s core level (in the process of increasing temperature) and the valence band of $La_{1-x}Sr_xMnO_3$ (x = 0.2, 0.3 and 0.4), $\Delta\mu$ for bilayered system $La_{2-2x}Sr_{1+2x}Mn_2O_7$ ($x = 0.4$) and correlated hopping model of Mn^{3+}/Mn^{4+} mixed-valence state as a function of temperature [6.13, 21, 22, 23, 24, 25]. We consider that the temperature-dependent shifts of the O 1s core level and the valence band for $La_{1-x}Sr_xMnO_3$ are ascribed to the temperature-dependent change in $\Delta\mu$. For NSMO and $La_{1-x}Sr_xMnO_3$, the $\Delta\mu$ curves show similar temperature dependences in the sense that the chemical potential is shifted upward with decreasing temperature. We consider that the shifts are understood in terms of the DE interaction (and possibly the temperature dependence of the splitting of the e_g band caused by the dynamical/local JT effect) [6.5, 6, 7, 12]. An upward chemical potential shift by applying magnetic field has also been observed in $La_{1-x}Sr_xMnO_3$, which may be ascribed to the DE interaction in the JT split e_g band [6.26]. However, the $\Delta\mu$ for the bilayered compound $La_{2-2x}Sr_{1+2x}Mn_2O_7$ reported by Schulte *et al.* [6.13] is opposite to the prediction of the DE model. They speculated that the two dimensionality might affect the temperature-dependent chemical potential shift, but its origin remains as an open question.

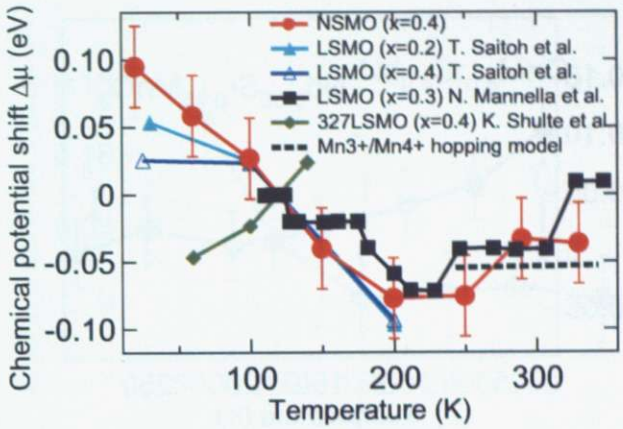

Figure 6.6: Comparison of the chemical potential shift $\Delta\mu$ in $Nd_{1-x}Sr_xMnO_3$ ($x = 0.4$) with the shifts of the O 1s core level (in the process of increasing temperature) and the valence band of $La_{1-x}Sr_xMnO_3$ ($x = 0.2$, 0.3 and 0.4 with $T_C \approx 310$, 370, and 370 K, respectively) [6.22, 21], $\Delta\mu$ for the bilayered system $La_{2-2x}Sr_{1+2x}Mn_2O_7$ ($x = 0.4$ with $T_C \approx 125$ K) [6.13] and correlated hopping model of Mn^{3+}/Mn^{4+} mixed-valence state. The spectral shifts have been translated to the chemical potential shift, assuming that the spectral shifts are primarily close to the chemical potential shift.

Also, we have compared the experimentally observed shifts with the results of the correlated hopping model in the splitting of the e_g band due to the dynamical/local JT distortion [6.23, 24, 25]. The correlated hopping model is given by $\Delta\mu = -k_B \ln\left(\frac{g_3}{g_4}\frac{x}{1-x}\right) \times T + \text{const.}$, where g_3 and g_4 are the spin-orbital degeneracies of Mn^{3+} and Mn^{4+}, respectively and x is the fraction of Mn^{4+} ions [6.23, 24, 25]. The parameters were fixed at $g_3 = 5$, $g_4 = 4$ and $x = 0.4$, corresponding to the Mn^{3+}/Mn^{4+} mixed-valence state in the split of the e_g band. We have plotted the calculated $\Delta\mu$ as shown by a dashed line in Fig. 6.6 [6.23, 24, 25]. The result is in qualitative agreement with the observed chemical potential shift in high-temperature region of NSMO with $x = 0.4$.

For other hole concentrations of NSMO, too, we confirmed that the observed temperature-dependent shifts were common to the O 1s, Sr 3d, Nd 3d and Mn 2p core levels and deduced the temperature-dependent chemical potential shifts by taking the average of the shifts of the four core levels. Figure 6.7 shows the $\Delta\mu$ for NSMO with $x = 0.45$ as a function of temperature. The shift $\Delta\mu$ was suppressed just below the T_C as in the case of $x = 0.4$, in accordance with the enhancement of the diffuse scattering due to

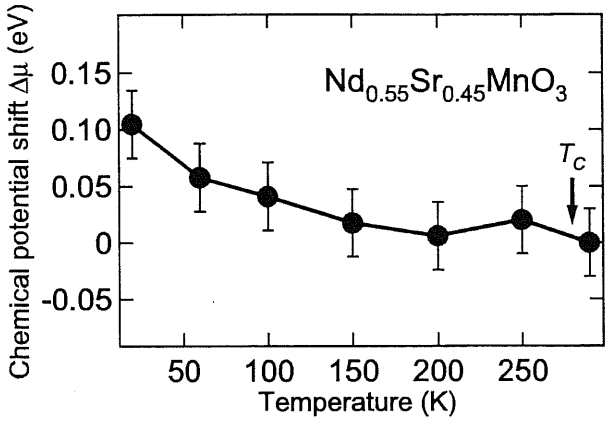

Figure 6.7: Chemical potential shift in $Nd_{0.55}Sr_{0.45}MnO_3$. T_C denotes Curie temperature.

the lattice polarons [6.5, 6, 7]. We attribute the shift in the low-temperature region of the FM phase for $x = 0.45$ to the DE interaction (and the temperature dependence of the splitting of the e_g band due to the dynamical/local JT effect) as in the case of $x = 0.4$. [6.5, 6, 7, 12]. The magnitude of the observed shift for $x = 0.45$ is smaller than that for $x = 0.4$, consistent with the one-orbital DE model resulting from the JT splitting [see Fig. 6.2(b)].

Figure 6.8 shows the $\Delta\mu$ for NSMO with $x = 0.5$ as a function of temperature. The large upward shift with decreasing temperature observed below the T_{CO} is attributed to the opening of a gap, as has been found for the CE-type CO phase of $Pr_{1-x}Ca_xMnO_3$ [6.27]. That is, if the chemical potential is located near the bottom of the upper band and the CO gap is gradually opened with decreasing temperature, the chemical potential would be shifted upward with decreasing temperature. Indeed, Kuwahara *et al.* [6.28] investigated the doping dependence of Seebeck coefficient in NSMO and found that the NSMO with $x = 0.5$ shows electron-type conduction. It has been reported from the studies of tunneling spectroscopy and photoemission spectroscopy that the CO gap of NSMO shows a temperature dependence [6.29, 30]. For the A-type AF metallic phase of NSMO with $x = 0.55$ and 0.6, we observed an upward chemical potential shifts with decreasing temperature as shown in Fig. 6.9(a) and 5.9(b), probably related to the nature of the two-dimensional metal. An upward shift with decreasing temperature was also observed for C-type AF insulating phase (see Fig. 6.9(c)).

In Fig. 6.10, we have summarized the chemical potential shift in NSMO as a function of temperature and hole concentration. In the case of the hole-

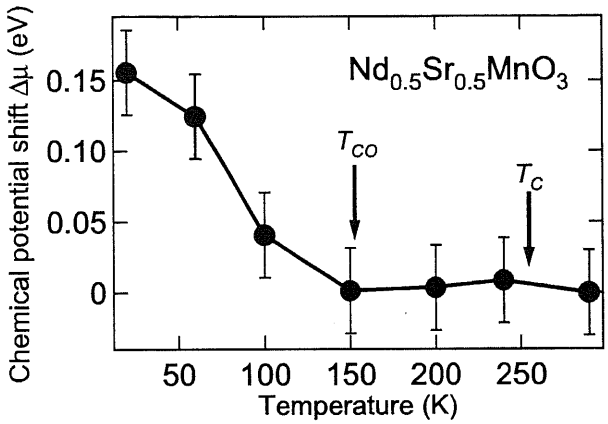

Figure 6.8: Chemical potential shift in $Nd_{0.5}Sr_{0.5}MnO_3$. T_C and T_{CO} denote Curie temperature and charge-ordering temperature, respectively.

concentration-dependent chemical potential shift, the shifts of only the Mn $2p$ core level was different from those of the O $1s$, Sr $3d$ and Nd $3d$ core levels because of the change of the chemical-shift term [6.20]. Therefore, we deduced the hole-concentration-dependent chemical potential shift by taking the average of the shifts of the O $1s$, Sr $3d$ and Nd $3d$ core levels. We found the suppression of the doping-dependent chemical potential shift near and in the CE-type CO composition range of NSMO as discussed in Chapter 5.

6.4 Conclusion

We have measured the chemical potential shift as a function of temperature in NSMO by means of core-level photoemission spectroscopy. We have found an anomalous upward chemical potential shift with decreasing temperature in the low-temperature region of the FM phase and its suppression in the high-temperature region of the FM phase near T_C. We attribute the large shift in the low-temperature region to the change of bandwidth due to the DE interaction (and possibly the temperature dependence of the splitting of the e_g level caused by the dynamical/local JT effect.) Also, the suppression of the shift at higher temperatures is ascribed to the influence of lattice-polaron formation. Furthermore, we observed an upward chemical potential shift with decreasing temperature in the CE-type AF charge-ordered, A-type AF metallic, and C-type AF insulating phases.

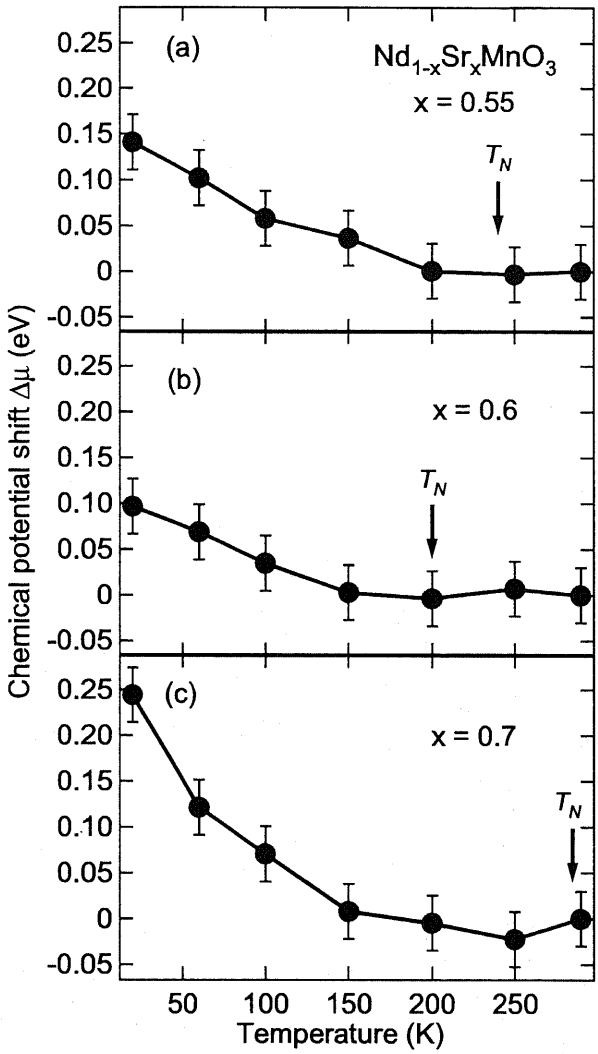

Figure 6.9: Chemical potential shifts in (a) $Nd_{0.45}Sr_{0.55}MnO_3$, (b) $Nd_{0.4}Sr_{0.6}MnO_3$ and (c) $Nd_{0.3}Sr_{0.7}MnO_3$. T_N denotes Néel temperature.

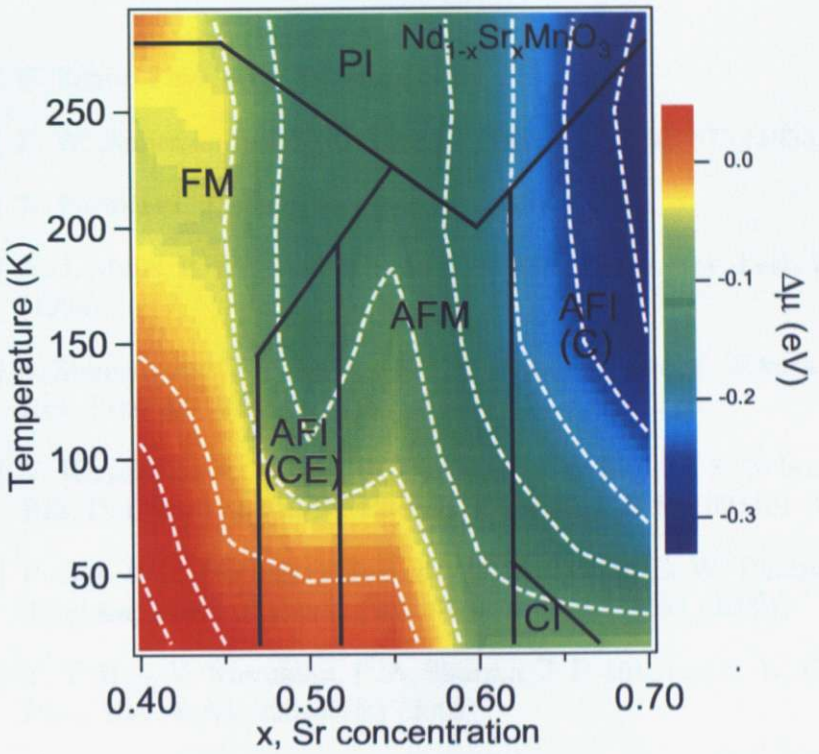

Figure 6.10: Summary of chemical potential shift $\Delta\mu$ in $Nd_{1-x}Sr_xMnO_3$ as a function of temperature and hole concentration. PI: Paramagnetic insulating phase; CI: Spin-canted insulating phase; FM: Ferromagnetic metallic phase; AFM: Antiferromagnetic metallic phase; AFI: Antiferromagnetic insulating phase [6.14, 15].

References

[6.1] C. Zener, Phys. Rev. **82**, 403 (1951).

[6.2] P. W. Anderson and H. Hasegawa, Phys. Rev. **100**, 675 (1955).

[6.3] N. Furukawa, J. Phys. Soc. Jpn. **63**, 3214 (1994).

[6.4] A. J. Millis, B. I. Shraiman, and R. Mueller, Phys. Rev. Lett. **77**, 175 (1996).

[6.5] S. Shimomura, N. Wakabayashi, H. Kuwahara, and Y. Tokura, Phys. Rev. Lett. **83**, 4389 (1999).

[6.6] V. Kiryukhin, T. Y. Koo, A. Borissov, Y. J. Kim, C. S. Nelson, J. P. Hill, D. Gibbs, and S.-W. Cheong, Phys. Rev. B **65**, 094421 (2002).

[6.7] P. Dai, J. A. Fernandez-Baca, N. Wakabayashi, E. W. Plummer, Y. Tomioka, and Y. Tokura, Phys. Rev. Lett. **85**, 2553 (2000).

[6.8] T. Y. Koo, V. Kiryukhin, P. A. Sharma, J. P. Hill, and S.-W. Cheong, Phys. Rev. B **64**, 220405(R) (2001).

[6.9] A. Lanzara, N. L. Saini, M. Brunelli, F. Natali, A. Bianconi, P. G. Radaelli, and S.-W. Cheong, Phys. Rev. Lett. **81**, 878 (1998).

[6.10] C. H. Booth, F. Bridges, G. H. Kwei, J. M. Lawrence, A. L. Cornelius, and J. J. Neumeier, Phys. Rev. Lett. **80**, 853 (1998).

[6.11] D. Louca, T. Egami, E. L. Brosha, H. Röder, and A. R. Bishop, Phys. Rev. B **56**, R8475 (1997).

[6.12] N. Furukawa, J. Phys. Soc. Jpn. **66**, 2523 (1997).

[6.13] K. Schulte, M. A. James, L. H. Tjeng, P. G. Steeneken, G. A. Sawatzky, R. Suryanarayanan, G. Dhalenne, and A. Revcolevschi, Phys. Rev. B **64**, 134428 (2001).

[6.14] H. Kuwahara, Y. Tomioka, Y. Moritomo, and Y. Tokura, Science **270**, 961 (1995).

[6.15] Y. Tokura, Rep. Prog. Phys **69**, 797 (2006).

[6.16] K. Horiba, M. Taguchi, A. Chainani, Y. Takata, E. Ikenaga, D. Miwa, Y. Nishino, K. Tamasaku, M. Awaji, A. Takeuchi, M. Yabashi, H. Namatame, M. Taniguchi, H. Kumigashira, M. Oshima, M. Lippmaa, M. Kawasaki, H. Koinuma, K. Kobayashi, T. Ishikawa, and S. Shin, Phys. Rev. Lett. **93**, 236401 (2004).

[6.17] K. Horiba, M. Taguchi, N. Kamakura, K. Yamamoto, A. Chainani, Y. Takata, E. Ikenaga, H. Namatame, M. Taniguchi, M. Awaji, A. Takeuchi, D. Miwa, Y. Nishino, K. Tamasaku, T. Ishikawa, H. Kumigashira, M. Oshima, M. Lippmaa, M. Kawasaki, H. Koinuma, K. Kobayashi, and S. Shin, J. Electron Spectrosc. Relat. Phenom. **144-147**, 557-559 (2005).

[6.18] K. Horiba, A. Chikamatsu, H. Kumigashira, M. Oshima, N. Nakagawa, M. Lippmaa, K. Ono, M. Kawasaki, and H. Koinuma, Phys. Rev. B **71**, 155420 (2005).

[6.19] J. Matsuno, A. Fujimori, Y. Takeda, and M. Takano, Europhys. Lett. **59**, 252 (2002).

[6.20] K. Ebata, H. Wadati, M. Takizawa, A. Fujimori, A. Chikamatsu, H. Kumigashira, M. Oshima, Y. Tomioka, and Y. Tokura, Phys. Rev. B **74**, 064419 (2006).

[6.21] T. Saitoh, A. Sekiyama, K. Kobayashi, T. Mizokawa, A. Fujimori, D. D. Sarma, Y. Takeda, and M. Takano, Phys. Rev. B **56**, 8836 (1997).

[6.22] N. Mannella, A. Rosenhahn, C. H. Booth, S. Marchesini, B. S. Mun, S.-H. Yang, K. Ibrahim, Y. Tomioka, and C. S. Fadley, Phys. Rev. Lett. **92**, 166401 (2004).

[6.23] Y. Ishida, H. Ohta, A. Fujimori, and H. Hosono, J. Phys. Soc. Jpn. **76**, 103709 (2007).

[6.24] P. M. Chaikin and G. Beni, Phys. Rev. B **13**, 647 (1976).

[6.25] W. Koshibae, K. Tsutsui, and S. Maekawa, Phys. Rev. B **62**, 6869 (2000).

[6.26] D. Wu, Z. H. Xiong, X. G. Li, Z. V. Vardeny, and J. Shi, Phys. Rev. Lett. **95**, 016802 (2005).

[6.27] K. Ebata, M. Hashimoto, K. Tanaka, A. Fujimori, Y. Tomioka, and Y. Tokura, Phys. Rev. B, **76**, 174418 (2007).

[6.28] H. Kuwahara, Y. Hirobe, J. Nagayama, S. Kodama, and A. Kakishima, J. Magn. Magn. Mater **272-276**, e1393 (2004)

[6.29] A. Biswas, A. K. Raychaudhuri, R. Mahendiran, A. Guha, R. Mahesh, and C. N. R. Rao, J. Phys.: Condens. Mat. **9**, L355 (1997).

[6.30] A. Sekiyama, S. Suga, M. Fujikawa, S. Imada, T. Iwasaki, K. Matsuda, T. Matsushita, K. V. Kaznacheyev, A. Fujimori, H. Kuwahara, and Y. Tokura, Phys. Rev. B **59**, 15528 (1999).

Chapter 7

Effects of filling and bandwidth control on the chemical potential in manganites

7.1 Introduction

Key features to understand the complex phase diagram as shown in Fig. 7.1 and the colossal magnetoresistance (CMR) of the perovskite-type manganites as a function of hole concentration and chemical pressure are the double-exchange (DE) interaction and the instabilities toward the spin, charge and orbital ordering [7.1, 2, 3, 4]. In this chapter, we have summarized the doping-dependent chemical potential shift of the small-bandwidth system $Pr_{1-x}Ca_xMnO_3$ (PCMO), the intermediate-bandwidth system $Nd_{1-x}Sr_xMnO_3$ (NSMO) and the large-bandwidth system $La_{1-x}Sr_xMnO_3$ (LSMO) by core-level photoemission spectroscopy and discussed the shifts as a function of both hole concentration and average A-site ionic radius $\langle r_A \rangle$. We observed the pinning of the chemical potential shift $\Delta\mu$ with hole concentration near and in the CE-type antiferromagnetic (AF) charge-ordered (CO) composition range and also found the shifts as a function of $\langle r_A \rangle$ induced by the orthorhombic distortion and the DE interaction.

7.2 Experimental

Single crystals of LSMO ($x = 0.2$, 0.3, 0.4, 0.45, 0.5, and 0.55) were prepared by the floating zone method [7.5]. These samples were supplied by Dr. Y. Tomioka and Prof. Y. Tokura of National Institute of Advanced Industrial Science and Technology. X-ray photoemission measurements were performed using a Mg $K\alpha$ source ($h\nu = 1253.6$ eV) and a SCIENTA SES-100 analyzer.

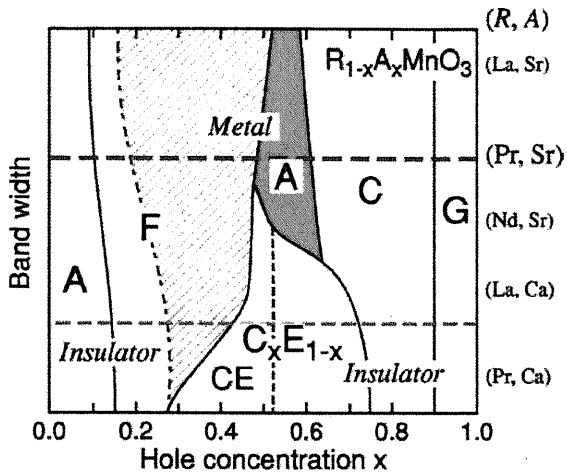

Figure 7.1: Schematic phase diagram of the perovskite-type $R_{1-x}A_x\mathrm{MnO}_3$ in the hole concentration-bandwidth plane at low temperatures. F, A, CE, C, and G denote ferromagnetic matallic, A-type antiferromagnetic, CE-type antiferromagnetic, C-type antiferromagnetic, and G-type antiferromagnetic phases, respectively [7.1, 2, 3, 4].

The energy resolution including the x-ray source and the analyzer was about 800 meV. The measured binding energies were stable, because the gold $4f_{7/2}$ core-level spectrum did not changed in the measurements with the accuracy of ± 10 meV. All the photoemission measurements were performed under the base pressure of $\sim 10^{-10}$ Torr at room temperature (RT). The sample surfaces were repeatedly scraped *in situ* with a diamond file to obtain clean surfaces. The cleanliness of the surfaces was checked by the weakness of contamination- or degradation-related feature on the higher binding energy side of the O 1*s* peak.

7.3 Results and discussion

Figure 7.2 shows the spectra of the O 1*s*, Sr 3*d*, La 3*d* and Mn 2*p* core levels at RT. The vertical lines mark the estimated positions of the core levels employed in the present study. For the O 1*s* core level, we used the midpoint of the lower binding energy side of the peak to estimate the core-level shift because the higher binding energy side of the O 1*s* peak is sensitive to surface contamination and degradation. We have also used the midpoint for the Sr 3*d* and La 3*d* core levels for the same reason. As for the Mn 2*p* core level, the peak position was used because the line shapes of the Mn

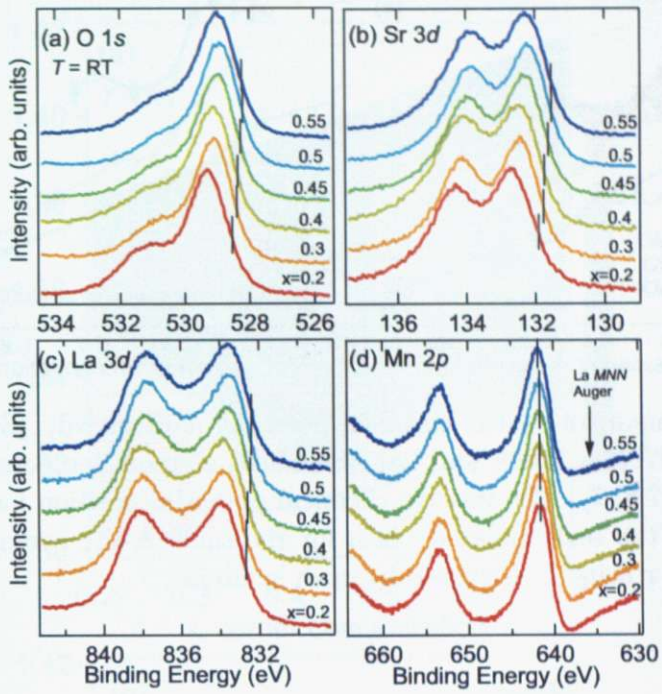

Figure 7.2: Core-level photoemission spectra of $La_{1-x}Sr_xMnO_3$ taken with the Mg $K\alpha$ line at room temperature. (a) O 1s; (b) Sr 3d; (c) La 3d; (d) Mn 2p. The intensity has been normalized to the peak height.

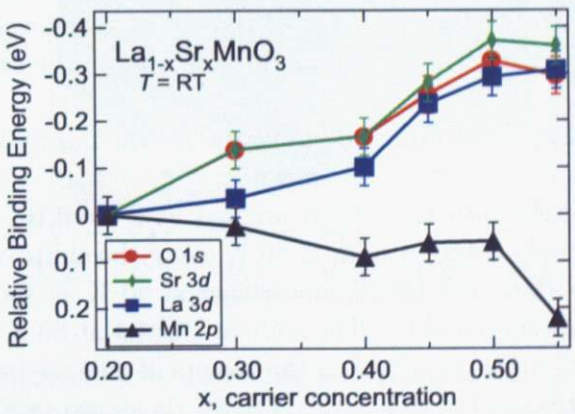

Figure 7.3: Binding energy shifts of the O 1s, Sr 3d, La 3d, and Mn 2p core levels as functions of carrier concentration x at room temperature.

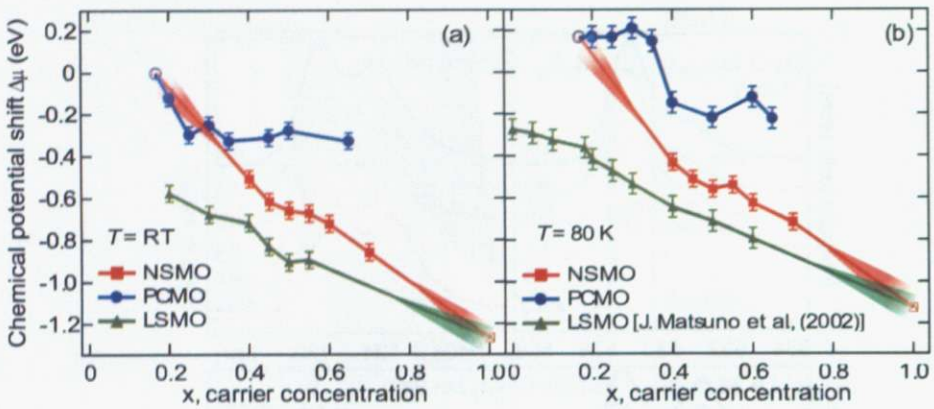

Figure 7.4: Comparison of the chemical potential shift in $Nd_{1-x}Sr_xMnO_3$ with those in $Pr_{1-x}Ca_xMnO_3$ and $La_{1-x}Sr_xMnO_3$ at room temperature (a) and 80 K (b). [7.6, 7]. The relative chemical potential position have been aligned so that the (extrapolated) data for the same A-site average ionic radius $\langle r_A \rangle$ and x coincide (denoted by open symbols).

$2p$ core levels slightly changed with composition and the midpoint position depended on the peak width.

In Fig. 7.3, the binding-energy shifts of the O $1s$, Sr $3d$, La $3d$ and Mn $2p$ core levels at RT are plotted. One can see the shifts of only the Mn $2p$ core level was different from those of the O $1s$, Sr $3d$ and La $3d$ core levels because of the change in the chemical-shift term [7.6]. Therefore, we deduced the doping-dependent chemical potential shift in LSMO by taking the average of the shifts of the O $1s$, Sr $3d$ and La $3d$ core levels as shown in Fig. 7.4(a) [7.6]. The $\Delta\mu$ of LSMO at RT was almost the same as that at $\sim$ 80 K [7.7].

We extrapolated each set of the $\Delta\mu$ data and set the $\Delta\mu$ for same A-site average ionic radius $\langle r_A \rangle$ identical as shown in Fig. 7.4(a). For example, the PCMO and NSMO data have been aligned at $x = 0.167$. We have also deduced the corresponding results at 80 K using the shifts of core-level spectra of LSMO, NSMO and PCMO measured at 80 K as shown in Fig. 7.4(b) [7.7] (see Chapters 3 and 6). The shift in PCMO at 80 K was strong in the CO region $x \lesssim 0.5$ as reported in the results of valence-band shift at 80 K in contrast to that in PCMO at RT [7.6, 8]. As shown in Fig. 7.4, the incommensurate charge modulation in PCMO exists in a wider range of the carrier concentration at RT than at 80 K as observed by electron diffraction or x-ray resonant scattering [7.9]. On the other hand, the suppression of the $\Delta\mu$ in PCMO at 80 K was observed in the CO region $x \gtrsim 0.5$. The shifts

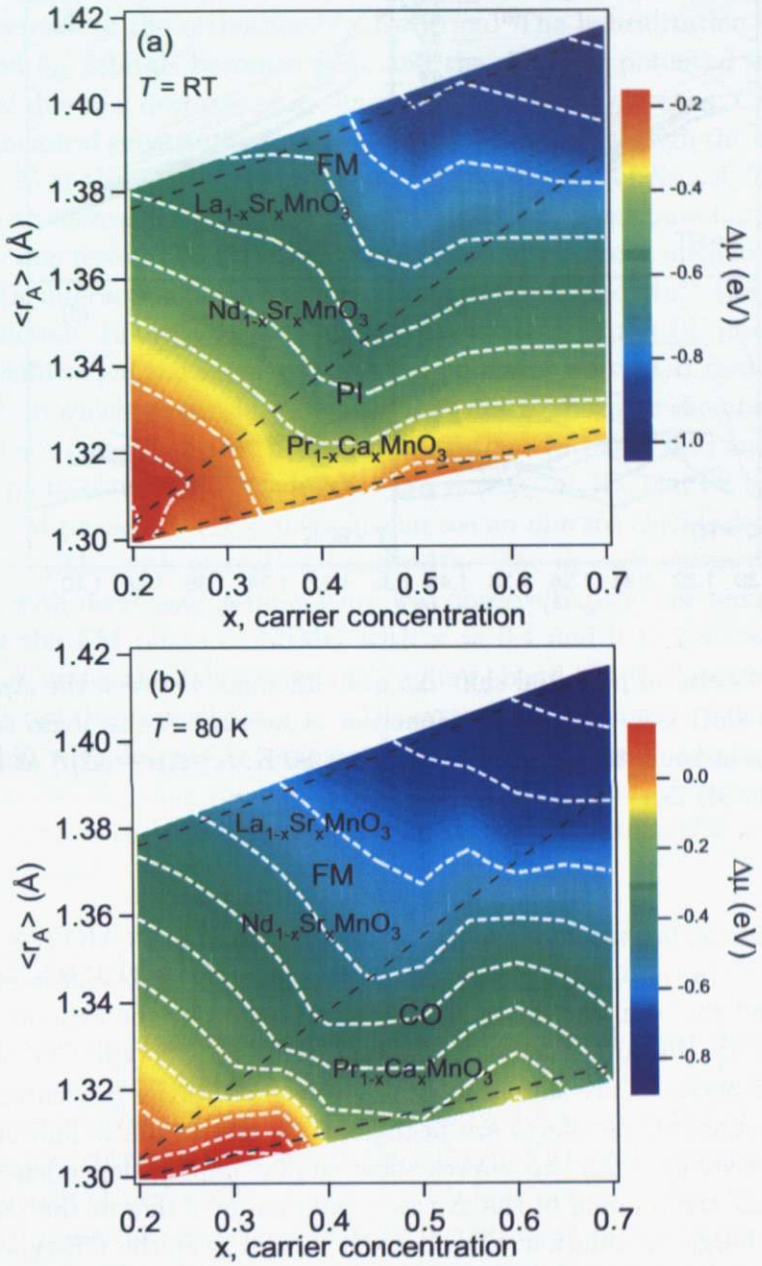

Figure 7.5: Chemical potential shift in $Pr_{1-x}Ca_xMnO_3$, $Nd_{1-x}Sr_xMnO_3$, and $La_{1-x}Sr_xMnO_3$ as a function of A-site average ionic radius $\langle r_A \rangle$ and x at room temperature (a) and 80 K (b) [7.4, 6, 7]. FM, PI and CO denote ferromagnetic metallic, paramagnetic insulating and charge-ordering phases, respectively.

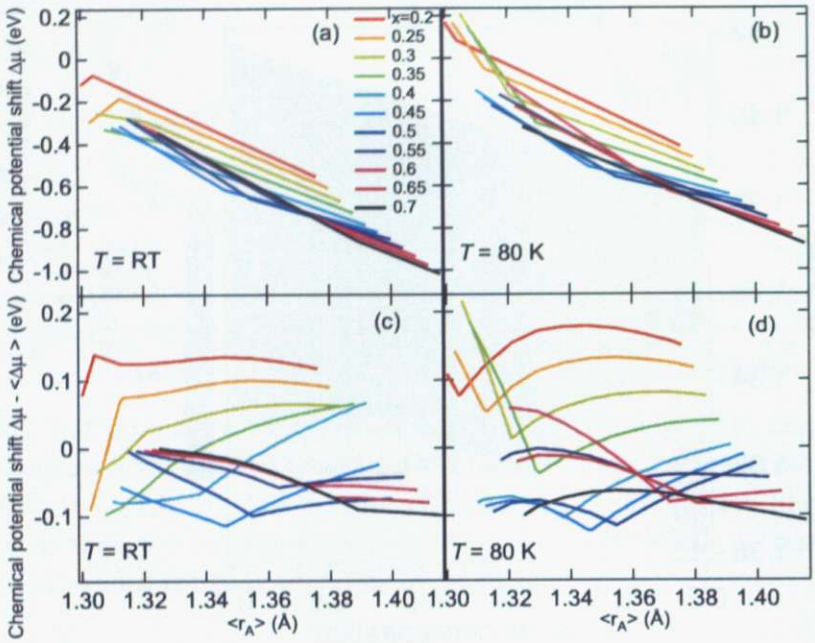

Figure 7.6: Chemical potential shift $\Delta\mu$ and difference between the $\Delta\mu$ and the average shift $\Delta\mu - \langle\Delta\mu\rangle$ as a function of average A-site ionic radius $\langle r_A\rangle$. (a) $\Delta\mu$ at room temperature; (b) $\Delta\mu$ at 80 K; (c) $\Delta\mu - \langle\Delta\mu\rangle$ at room temperature; (d) $\Delta\mu - \langle\Delta\mu\rangle$ at 80 K.

with x reflect the evolution of the periodicity of stripes in PCMO [7.8, 9].

Figure 7.5(a) and 7.5(b) show $\Delta\mu$ in the plane of $\langle r_A\rangle$ and x at RT and 80 K and the resulting $\Delta\mu$ is linearly interpolated by the experimental data [7.4, 6, 7]. In large-bandwidth systems with no CE-type CO phase, the chemical potential are shifted monotonously with carrier concentration, probably because stripe effects are negligible. In intermediate- and small-bandwidth systems, both $\Delta\mu$ curves show similar doping dependences in the sense that the pinning of the $\Delta\mu$ as a function of x due to the incommensurate charge modulation was observed in and near the CE-type CO composition range. The clear difference in the doping dependence of the chemical potential shifts reflects the existence and absence of the CE-type CO phase. The results thus indicate that the tendency toward charge self-organization around $x \sim 0.5$ such as stripe formation is indeed enhanced with decreasing bandwidth.

We note that a downward chemical potential shift was generally observed with increasing $\langle r_A\rangle$ at RT and 80 K as shown in Fig. 7.6(a) and

7.6(b). The overall downward shift with increasing $\langle r_A \rangle$ may be related to the decrease of the orthorhombic distortion. The hybridization between the e_g and t_{2g} orbitals becomes weak and the chemical potential is shifted downward due to a decrease of the energy level of the e_g electons. Change of $\langle r_A \rangle$ by chemical substitutions gives bandwidth control through the chemical pressure. Note that if x is fixed constant, the bandwidth of $R_{1-x}A_xMnO_3$ increases with increasing $\langle r_A \rangle$. The large-bandwidth systems have been known as conducting ferromagnets, where the itinerant e_g electrons mediate the ferromagnetic interaction between the neighboring Mn^{3+} and Mn^{4+} through the DE interaction. In order to estimate the $\Delta\mu$ induced by the DE interaction, we have subtracted the averaged chemical potential shift $\langle \Delta\mu \rangle$ from the $\Delta\mu$ with $\langle r_A \rangle$, in which we consider that the shift due to the orthorhombic distortion does not depend on the carrier concentration. In Fig. 7.6(c) and 7.6(d), we have plotted the subtracted shifts $\Delta\mu - \langle \Delta\mu \rangle$ at RT and 80 K. In the range of FM phase $0.3 < x < 0.5$, one can see an upward chemical potential shift $\Delta\mu - \langle \Delta\mu \rangle$ with increasing bandwidth. The upward chemical potential shift with decreasing temperature was observed in the low-temperature region of the FM phase of NSMO with $x = 0.4$ and 0.45 because of DE interaction under the Jahn-Teller (JT)-split e_g band [7.10]. Furukawa [7.11] has predicted theoretically that in a DE system a large upward chemical potential shift with decreasing temperature in the FM phase due to the change of the bandwidth using the one-orbital model. Therefore, we attribute the upward shifts with increasing bandwidth to the DE interaction under the JT-split e_g band.

7.4 Conclusion

We have experimentally determined the doping and band-width dependences of the chemical potential in LSMO, NSMO, and PCMO by means of core-level photoemission spectroscopy. We observed a suppression of the shift with hole concentration near and in the CE-type CO composition range due to the change of periodicity of stripes with hole doping. Also, we found a downward chemical potential shift with increasing $\langle r_A \rangle$ due to the decrease of the orthorhombic distortion. After subtracting the shift induced by the orthorhombic distortion, an upward chemical potential shift with increasing bandwidth was realized in the region of FM phase $0.3 < x < 0.5$, which we attribute this shift to the DE interaction in the JT-split e_g band.

References

[7.1] R. Kajimoto, H. Yoshizawa, Y. Tomioka, and Y. Tokura, Phys. Rev. B **66**, 180402(R) (2002).

[7.2] H. Kuwahara, Y. Tomioka, Y. Moritomo, and Y. Tokura, Science **270**, 961 (1995).

[7.3] Y. Tomioka, A. Asamitsu, H. Kuwahara, Y. Moritomo, and Y. Tokura, Phys. Rev. B **53**, 1689 (1996).

[7.4] Y. Tokura, Rep. Prog. Phys **69**, 797 (2006).

[7.5] A. Urushibara, Y. Moritomo, T. Arima, A. Asamitsu, G. Kido, and Y. Tokura, Phys. Rev. B **51**, 14103 (1995).

[7.6] K. Ebata, H. Wadati, M. Takizawa, A. Fujimori, A. Chikamatsu, H. Kumigashira, M. Oshima, Y. Tomioka, and Y. Tokura, Phys. Rev. B **74**, 064419 (2006).

[7.7] J. Matsuno, A. Fujimori, Y. Takeda, and M. Takano, Europhys. Lett. **59**, 252 (2002).

[7.8] K. Ebata, M. Hashimoto, K. Tanaka, A. Fujimori, Y. Tomioka, and Y. Tokura, Phys. Rev. B **76**, 174418 (2007).

[7.9] G. C. Milward, M. J. Calderon, and P. B. Littlewood, Nature **433**, 607 (2005).

[7.10] K. Ebata, M. Takizawa, K. Maekawa, A. Fujimori, H. Kuwahara, Y. Tomioka, and Y. Tokura, cond-mat 07104462 (2007).

[7.11] N. Furukawa, J. Phys. Soc. Jpn. **66**, 2523 (1997).

Chapter 8

Observation of photoinduced effects in manganites studied by x-ray photoemission spectroscopy

8.1 Introduction

The CE-type antiferromagnetic (AF) charge-ordered (CO) state is energetically nearly degenerate with the ferromagnetic metallic (FM) state, in which double-exchange interaction dominates [8.1]. The phase transition from the CE-type CO phase to the FM phase can be driven by external stimuli such as light illumination [8.2, 3], magnetic field [8.4], and electric field [8.5]. Photo-induced phase transitions observed in the manganites are interesting in terms of creating novel optoelectric devices. Miyano *et al.* [8.2] succeeded in inducing an insulator-to-metal transition in $Pr_{1-x}Ca_xMnO_3$ (PCMO) by the illumination of laser pulses in cooperation with an electric field. It has been considered that photoexcited carriers make the CE-type CO state collapse, and FM domain produces a continuous conducting paths under the application of electric field as shown in Fig 8.1(a) [8.3, 6]. Here, the CE-type CO state in PCMO is stabilized in the wide hole concentration range between $x \simeq 0.3$ and 0.75 because of its small bandwidth [8.4, 7]. In a recent photoemission study of PCMO, we have observed the opening of an energy gap near the Fermi level (E_F) below the CO transition temperature and a downward chemical potential shift ($\Delta\mu$) with increasing temperature [8.8]. A large drop of the resistivity has been observed in $Pr_{1-x}(Ca_{1-y}Sr_y)_xMnO_3$ thin film by light illumination even without any assisting electronic field as shown in Fig. 8.1(b) [8.9, 10]. In an x-ray photoemission spectroscopy (XPS)

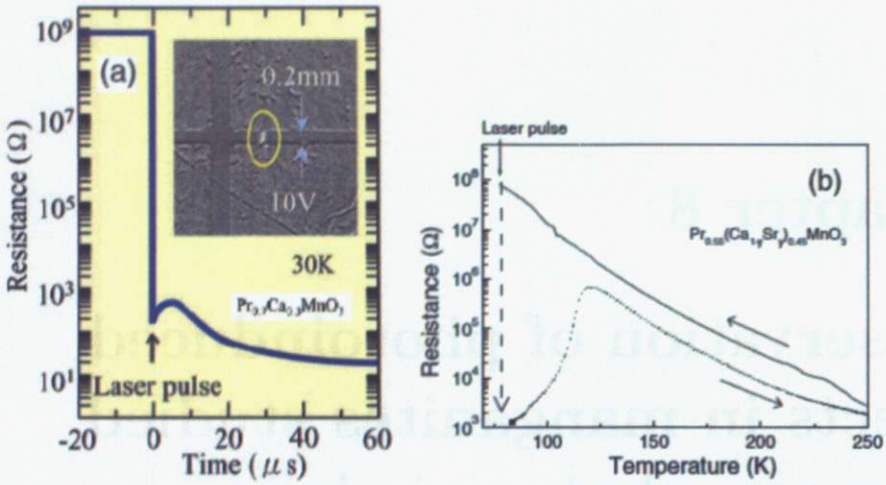

Figure 8.1: Photo-induced insulator-to-metal transition in manganites [8.1, 3, 9, 10]. (a) Resistance change in $Pr_{1-x}Ca_xMnO_3$ with $x = 0.3$ upon the 7 ns pulse laser irradiation for a voltage of 10 V applied to the sample electrodes separated by a 0.2 mm gap. Inset represents the region of the current path [8.1, 3]. (b) Temperature dependence of resistance for $Pr_{1-x}(Ca_{1-y}Sr_y)_xMnO_3$ thin film with $x = 0.45$ and $y = 0.25$. The irradiation of 100 laser pulses brings the large drop of resistance (dashed line with downward arrow) [8.9, 10].

study of $Pr_{1-x}(Ca_{1-y}Sr_y)_xMnO_3$ thin film, enhancement of spectral weight at the Fermi level (E_F) was observed after laser illumination, indicating the increase of the FM volume fraction [8.11]. Okimoto *et al.* [8.12] observed a persisitent increase of magnetization by photoexcitation in 1 % Cr-doped PCMO thin film.

It has also been reported that a suppression of ferromagnetic spin correlation occurs in the FM phase of manganites when the down-spin Mn $3d$ electrons are photo-excited. Matsuda *et al.* [8.13] found an increase of the spectral weight of interband transition between the exchange-split e_g bands in the FM phase of $(Nd_{0.5}Sm_{0.5})_{0.6}Sr_{0.4}MnO_3$ thin film and ascribed it to a photo-induced demagnetization. Liu *et al.* [8.14, 15] observed changes in transmission and resistivity in the FM phase of $La_{0.6}Sr_{0.4}MnO_3$ due to the excitation of down-spin Mn $3d$ electrons. It has been shown by XPS that $Nd_{1-x}Sr_xMnO_3$ (NSMO) exhibits a large chemical potential shift with increasing temperature in the low-temperature region of the FM phase because of a change in the width of the Jahn-Teller-split e_g band induced by double-exchange mechanism as discussed in Chapter 6 [8.16].

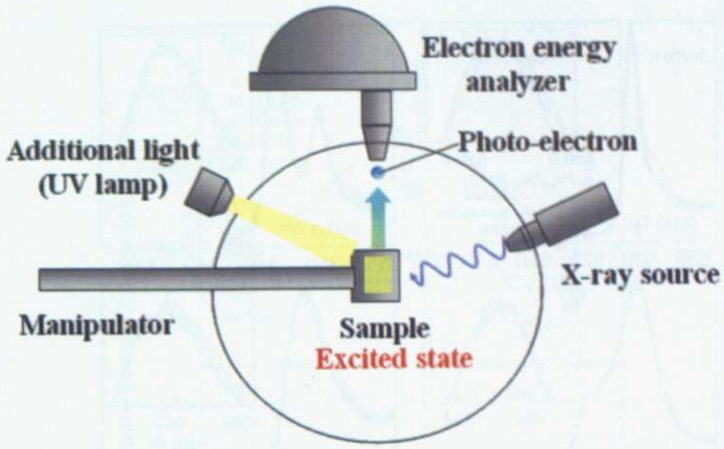

Figure 8.2: Schematic picture of the experimental setup.

In the present work, we have performed XPS measurements on PCMO with $x = 0.3$ and NSMO with $x = 0.4$ under light illumination and observed reversible chemical potential shifts in PCMO and NSMO that can be ascribed to the effect of photoexcitation. Spectral weight at E_F was enhanced under light illumination in the CE-type CO phase but not in the paramagnetic insulating (PI) phase of the PCMO, consistent with the photo-induced mechanism described above.

8.2 Experimental

Single crystals of PCMO with the carrier concentration of $x = 0.3$ and those of NSMO with the carrier concentration of $x = 0.4$ were grown by the floating-zone method. The growth techniques and the physical properties of the crystals were described in Refs.[8.4, 17]. These samples were supplied by Dr. Y. Tomioka and Prof. Y. Tokura of National Institute of Advanced Industrial Science and Technology and Prof. H. Kuwahara of Sophia University. XPS measurements were performed using the Mg $K\alpha$ source ($h\nu = 1253.6$ eV). All the photoemission measurements were performed under the base pressure of $\sim 10^{-10}$ Torr at 15-300 K. The samples were repeatedly scraped *in situ* with a diamond file to avoid surface contamination and degradation. The cleanliness of the sample surfaces was checked by monitoring the contamination/degradation-related features on the higher-binding-energy side of the O $1s$ core level. Photoelectrons were collected using a Scienta SES-100 electron-energy analyzer. The energy resolution including the light source was about 800 meV. The stability of the

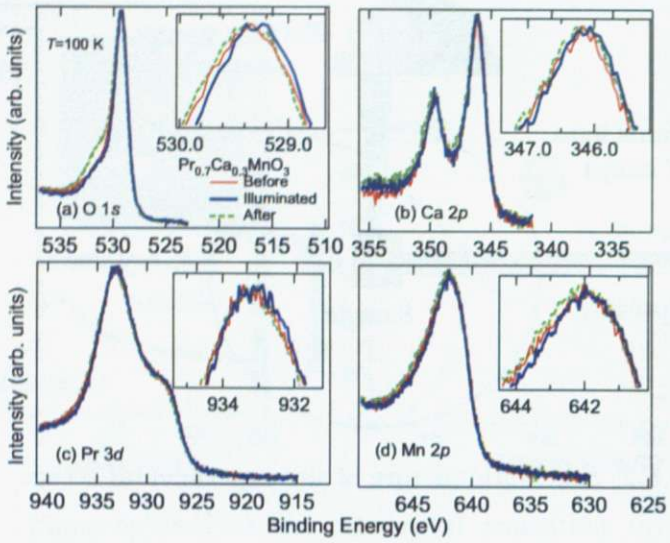

Figure 8.3: Core-level photoemission spectra of $Pr_{1-x}Ca_xMnO_3$ taken with $h\nu = 1253.6$ eV before, during and after light illumination at 100 K. (a) O $1s$; (b) Ca $2p$; (c) Pr $3d$; (d) Mn $2p$.

measured binding energies was confirmed by measuring the gold $4f_{7/2}$ core-level spectrum within the accuracy of ± 10 meV at each temperature. A Xe discharge lamp was used as the excitation light source and provided the light with $\lambda = 280$-400 nm, which almost coincides with the charge-transfer optical transition energy from the O $2p$ band to the Mn $3d$ $t_{2g\downarrow}$ and Mn $3d$ $e_{g\downarrow}$ states [8.14]. A schematic picture of experimental setup is shown in Fig. 8.2. The light intensity at the sample position was ~ 8 mW/cm^2. We confirmed that the increase of temperature at the sample position measured under light illumination did not exceed 1.5 K.

8.3 Results and discussion

8.3.1 $Pr_{1-x}Ca_xMnO_3$

Figure 8.3 shows the photoemission spectra of the O $1s$, Ca $2p$, Pr $3d$, and Mn $2p$ core levels in PCMO with $x = 0.3$ at 100 K under light illumination. All the core-level spectra are shifted toward lower binding energies when light was illuminated. In order to estimate the magnitudes of the shifts under light illumination, we have used the midpoint of the low binding-energy slope for the O $1s$ core level because the line shape on the higher

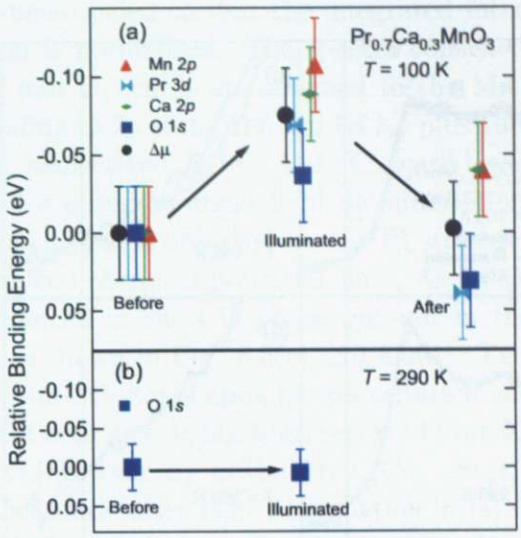

Figure 8.4: Core-level shifts in $Pr_{0.7}Ca_{0.3}MnO_3$ before, during and after light illumination at 100 K (a) and 290 K (b).

binding energy side of the O 1s spectra is sensitive to surface contamination or degradation. We have also used the midpoint method for the Ca 2p and Mn 2p core levels. As for Pr 3d core level, 70 % of the peak height of the low binding-energy slope was employed because the line shape near the midpoint on the lower-binding energy side slightly changed under light illumination.

In Fig. 8.4(a), we have plotted the binding energy shift of each core level in the CO phase at 100 K for PCMO with $x = 0.3$ under light illumination. One can see that the observed shifts were approximately common to all the core levels. Therefore, we interpret the core-level shifts shown in Fig. 8.4(a) as due to the chemical potential shift and take the average of the shifts of the four core levels as a measure of $\Delta\mu$. We consider that the photo-induced chemical potential shift is an intrinsic effect and not due to surface degradation or heating effect because the shift was reversible and the increase of temperature measured under light illumination did not exceed 1.5 K. Once the light was turn off, all the core levels went back to the initial energy positions. At 290 K, i.e., in the high-temperature PI phase, on the contrary, no photo-induced chemical potential shift was found as shown in Fig. 8.4(b).

The valence-band spectra of PCMO with $x = 0.3$ at 100 and 290 K under light illumination are shown in Fig. 8.5(a) and 8.5(b), respectively.

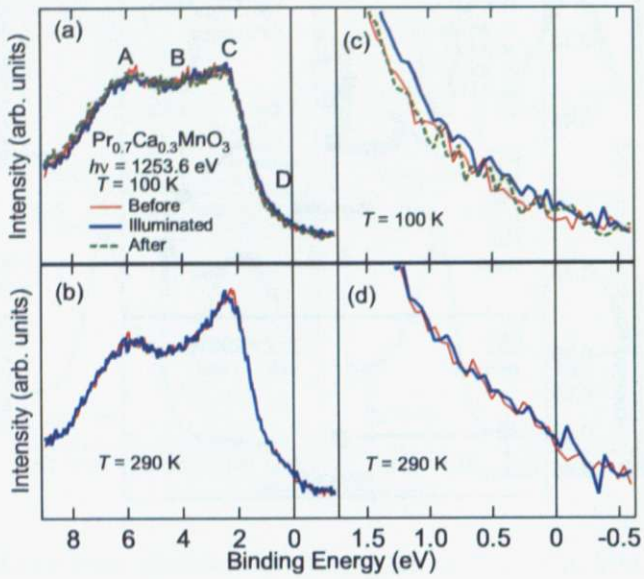

Figure 8.5: Valence-band photoemission spectra of $Pr_{0.7}Ca_{0.3}MnO_3$ before, during and after light illumination in the CO ($T = 100$ K) and PI ($T = 290$ K) phases taken with $h\nu = 1253.6$ eV. Entire valence band at 100 K (a) and 290 K (b); Spectra near E_F at 100 K (c) and 290 K (d).

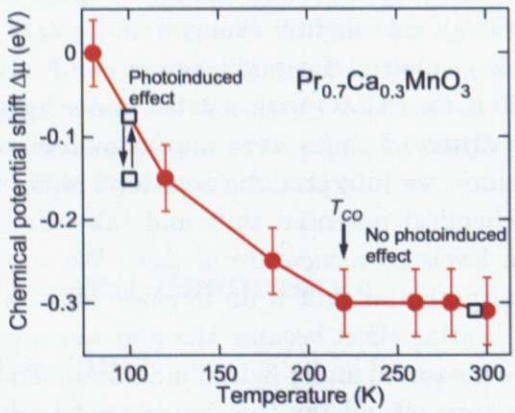

Figure 8.6: Photo-induced chemical potential shift at 100 and 290 K plotted with the temperature-dependent chemical potential shift in $Pr_{0.7}Ca_{0.3}MnO_3$ [8.8]. T_{CO} denotes the charge-ordering temperature.

The spectra have been scaled so that the integrated intensity in the entire valence-band region is normalized. The spectra consisted of structures labeled as A, B, C, and D, which are assigned to the Mn $3d$-O $2p$ bonding state, the non-bonding O $2p$ state, the Mn $3d$ t_{2g} plus the Pr $4f$ states and the Mn $3d$ e_g state, respectively [8.18]. A shift toward lower-binding energies of the valence band is observed under light illumination in the CO phase at 100 K while no such a shift is observed for the PI state at 290 K, consistent with the photo-induced chemical potential shift. As for the spectral weight near E_F, it is enhanced in the CO phase but not in the PI phase under light illumination as shown in Fig. 8.5(c) and 8.5(d). The results suggest a partial meltiing of the CO states upon photoexcitation and creation of local formation of the FM domains. It has been reported from XPS measurements that the spectral weight near E_F in the $Pr_{1-x}(Ca_{1-y}Sr_y)_xMnO_3$ thin film is enhanced in the CO phase after light illumination [8.11].

Fiebig *et al.* [8.3] observed a photo-induced insulator-to-metal transition in PCMO with $x = 0.3$ with assisting electric field. They also reported a temporal evolution of the reflectivity change in the same sample using pump-and-probe spectroscopy, indicating the melting of the CO phase induced by excited electrons [8.6]. We consider the $\Delta\mu$ under light illumination to be related to the melting of the CO phase by the excited electrons.

There has not been any report that the light illumination without any external field can stabilize the FM state in PCMO. On the other hand, in a recent work on $Pr_{1-x}(Ca_{1-y}Sr_y)_xMnO_3$ thin film, it has been reported that the FM state is stabilized by light illumination without any assisting external field [8.9]. In a theoretical study which takes into account the double-exchange interaction and Jahn-Teller distortion, it has been shown that the energy of the CO state is always lower than that of the FM phase in PCMO, while either FM or CO phase becomes stable for $Pr_{1-x}(Ca_{1-y}Sr_y)_xMnO_3$ in a reasonable parameter range [8.19].

The temperature-dependent chemical potential shift in PCMO has been deduced from the shift of the valence-band photoemission spectra in Ref.[8.8] as shown in Fig. 8.6. The upward chemical potential shift occurs with decreasing temperature due to the opening of the CO gap [8.8]. In Fig. 8.6, we have plotted the photo-induced chemical potential shift with the results of the temperature-dependent chemical potential shift in PCMO with $x = 0.3$. One can see the reversible chemical potential shift in the CO phase. The CO phase can be controlled by light illumination as well as temperature.

8.3.2 $Nd_{1-x}Sr_xMnO_3$

In Fig. 8.7, we have plotted the spectra of the O 1*s*, Sr 3*d*, Nd 3*d*, and Mn 2*p* core levels in the FM phase of NSMO with $x = 0.4$ at 15 K under light illumination. We have employed the midpoint of the low binding-energy side for the O 1*s*, Sr 3*d* and Mn 2*p* core levels to evaluate the core-level shifts. As for the Nd 3*d* core level, 80 % of the peak height of the low binding-energy slope was used because the line shape near the midpoint on the lower-binding energy side slightly changed under light illumination.

Figure 8.8(a) shows the binding energy shift of each core level in the FM phase under light illumination. One can see that the O 1*s*, Sr 3*d*, Nd 3*d*, and Mn 2*p* core levels are shifted in the same direction. Therefore, we take the average of the shifts of the four core levels as a measure of $\Delta\mu$, as in the case of PCMO. The chemical potential is shifted downward when the light is illuminated. After the light was turned off, all the core levels came back to the initial energy positions as shown in Fig. 8.8(a). On the other hand, we did not observe a photo-induced chemical potential shift in the high-temperature PI phase (see Fig. 8.8(b)). One can see that the photo-induced phase transition is observed in the FM phase but not in the PI phase. Valence-band spectra of NSMO in the FM and PI phases under light illumination are shown in Fig. 8.9. The spectra have been scaled so that the integrated intensity in the entire valence-band region is normalized. The valence band is shifted toward lower binding energies in the FM phase under light illumination, but not in the PI phase, consistent with the results of the core-level shifts.

An increase of spectral weight of the interband transition between the exchange-split e_g bands has been observed in the FM phase of Sm-doped NSMO thin film by the excitation of the down-spin Mn 3*d* electrons from O 2*p* band [8.13]. Liu *et al.* [8.14] have shown that a transient transmission change caused by the down-spin electrons occurs in the FM phase of $La_{1-x}Sr_xMnO_3$ thin film at room temperature. They have also observed a resistivity change induced by the down-spin electrons in $La_{1-x}Sr_xMnO_3$ thin film [8.15]. Therefore, we consider the chemical potential shift in the FM phase of NSMO to be connected with the photo-induced suppression of the ferromagnetic spin correlation.

The downward shift of the chemical potential with increasing temperature has been observed in the low-temperature region of the FM phase of NSMO due to double-exchange interaction in the Jahn-Teller-split e_g band [8.16]. We have plotted the observed shift under light illumination with the results of temperature-dependent chemical potential shift in NSMO with $x = 0.4$ as shown in Fig. 8.10 [8.16]. Note that the present shift under

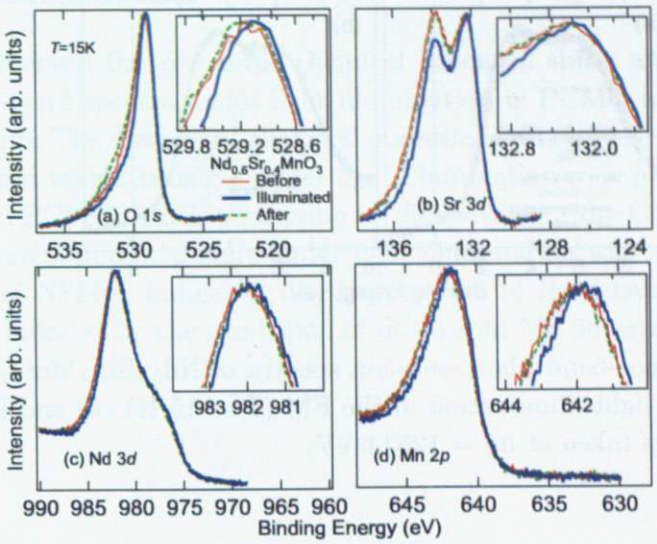

Figure 8.7: Core-level photoemission spectra of $Nd_{0.6}Sr_{0.4}MnO_3$ taken at $h\nu = 1253.6$ eV before, during and after light illumination at 15 K. (a) O 1*s*; (b) Sr 3*d*; (c) Nd 3*d*; (d) Mn 2*p*.

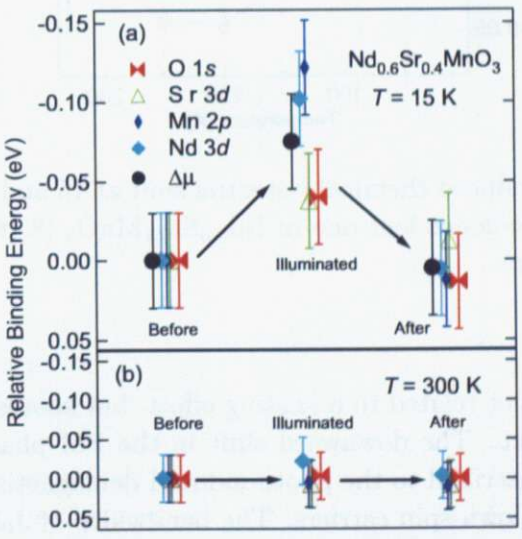

Figure 8.8: Core-level shifts in $Nd_{0.6}Sr_{0.4}MnO_3$ before, during and after light illumination at 15 K (a) and 300 K (b).

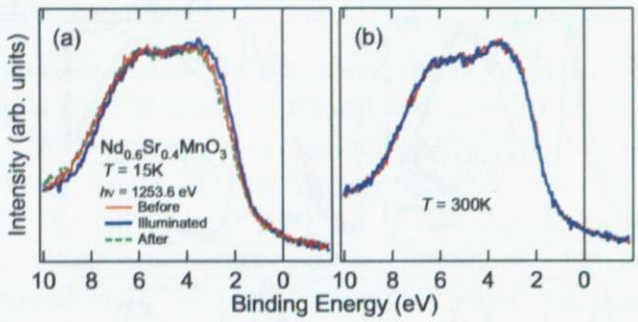

Figure 8.9: Valence-band photoemission spectra of $Nd_{0.6}Sr_{0.4}MnO_3$ before, during and after light illumination in the FM (T = 15 K) (a) and PI (T = 300 K) (b) phases taken at $h\nu$ = 1253.6 eV.

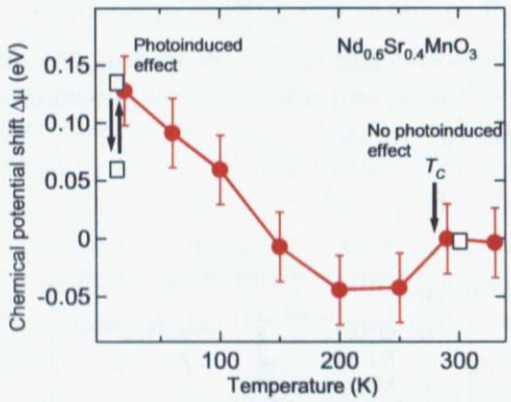

Figure 8.10: Photo-induced chemical potential shift at 15 and 300 K plotted with the temperature-dependent one in $Nd_{0.6}Sr_{0.4}MnO_3$ [8.16]. T_C denotes the Curie temperature.

light illumination is not related to a heating effect, but should be related to a photo-induced effect. The downward shift in the FM phase under light illumination can be ascribed to the photo-induced demagnetization induced by excitation of the down-spin carriers. The bandwidth of Jahn-Teller-split e_g electron becomes narrower due to the photo-induced demagnetization, which will lead to the downward shift of chemical potential.

8.4 Conclusion

We have observed the reversible chemical potential shifts and changes in the valence-band spectra under light illumination in PCMO and NSMO by means of XPS. The downward chemical potential shift and the enhancement of the spectral weight near E_F under light illumination were observed in the CO phase of PCMO, which we ascribe to the melting of the CO state. Also, a large chemical potential shift under light illumination was realized in the FM phase of NSMO, indicating the suppression of the ferromagnetic-spin correlation induced by the excitation of down-spin Mn $3d$ carriers.

References

[8.1] Y. Tokura, Rep. Prog. Phys **69**, 797 (2006).

[8.2] K. Miyano, T. Tanaka, Y. Tomioka, and Y. Tokura, Phys. Rev. Lett. **78**, 4257 (1997).

[8.3] M. Fiebig, K. Miyano, Y. Tomioka, and Y. Tokura, Science **280**, 1925 (1998).

[8.4] Y. Tomioka, A. Asamitsu, H. Kuwahara, Y. Moritomo, and Y. Tokura, Phys. Rev. B **53**, 1689 (1996).

[8.5] A. Asamitsu, Y. Tomioka, H. Kuwahara, and Y. Tokura, Nature **388**, 50 (1997).

[8.6] M. Fiebig, K. Miyano, Y. Tomioka, and Y. Tokura, Appl. Phys. B **71**, 211 (2000).

[8.7] Z. Jirak, S. Krupica, Z. Simsa, M. Dlouha, and S. Vratislav, J. Magn. Magn. Mater **53**, 153 (1985).

[8.8] K. Ebata, M. Hashimoto, K. Tanaka, A. Fujimori, Y. Tomioka, and Y. Tokura, Phys. Rev. B **76**, 174418 (2007).

[8.9] N. Takubo, Y. Ogimoto, M. Nakamura, H. Tamaru, M. Izumi, and K. Miyano, Phys. Rev. Lett. **95**, 017404 (2005).

[8.10] K. Miyano and N. Takubo, J. Phys. IV France **131**, 43-47 (2005).

[8.11] K. Takubo, J.-Y. Son, T. Mizokawa, N. Takubo, and K. Miyano, Phys. Rev. B **75**, 052408 (2007).

[8.12] Y. Okimoto, Y. Ogimoto, M. Matsubara, Y. Tomioka, T. Kageyama, T. Hasegawa, H. Koinuma, M. Kawasaki, and Y.Tokura, Appl. Phys. Lett. **80**, 1031 (2002).

[8.13] K. Matsuda, A. Machida, Y. Moritomo, and A. Nakamura, Phys. Rev. B **58**, R4203 (1998).

[8.14] X. Liu, A. Machida, Y. Moritomo, M. Ichida, and A. Nakamura, Jpn. J. Appl. Phys. **39**, L670 (2000).

[8.15] X. Liu, Y. Moritomo, A. Nakamura, and H. Asano, Jpn. J. Appl. Phys. **39**, L1233 (2000).

[8.16] K. Ebata, M. Takizawa, K. Maekawa, A. Fujimori, H. Kuwahara, Y. Tomioka, and Y. Tokura, cond-mat 07104462 (2007).

[8.17] H. Kuwahara, Y. Tomioka, Y. Moritomo, and Y. Tokura, Science **270**, 961 (1995).

[8.18] K. Ebata, H. Wadati, M. Takizawa, A. Fujimori, A. Chikamatsu, H. Kumigashira, M. Oshima, Y. Tomioka, and Y. Tokura, Phys. Rev. B **74**, 064419 (2006).

[8.19] L. Hao, J. Wang, and D. Y. Xing, Phys. Rev. B **74**, 014440 (2006).

Chapter 9

Summary and future prospects

In the preceding chapters, we have presented photoemission results on mixed-valence manganites $Pr_{1-x}Ca_xMnO_3$ (PCMO), $Nd_{1-x}Sr_xMnO_3$ (NSMO), and $La_{1-x}Sr_xMnO_3$ (LSMO), where the charge self-organization is thought to play a significant role in complex phenomena such as colossal magnetoresistance (CMR) and spin, charge, and orbital ordering. Our main findings are summarized as follows.

In Chapter 3, we have studied the chemical potential shift and changes in the electronic density of states near the Fermi level (E_F) as a function of carrier concentration in PCMO ($0.2 \leq x \leq 0.65$) through the measurements of photoemission spectra. The shift was suppressed for $x \gtrsim 0.5$ and was recovered for $x \lesssim 0.5$ in the low-temperature CE-type antiferromagnetic (AF) charge-ordered (CO) phase. In the high-temperature paramagnetic insulating (PI) phase, the suppression of the shift was observed near and in the CE-type CO composition range. We consider this observation to be related to the evolution of the periodicity of stripes or its fluctuations with hole doping. Together with the previous observation of monotonous chemical potential shift in LSMO, we conclude that the tendency toward the charge self-organization increases with decreasing bandwidth. In the valence band, spectral weight of the Mn $3d$ e_g electrons in PCMO was transferred from $\sim$ 1 eV below E_F to the region near E_F with hole doping, leading to a finite intensity at E_F even in the PI phase for $x \gtrsim 0.3$, probably related with the tendency toward charge self-organization. The finite intensity at E_F in spite of the insulating transport behavior is consistent with fluctuations involving ferromagnetic metallic (FM) states.

In Chapter 4, we have described the temperature dependence of the photoemission spectra of PCMO with $x = 0.25$, 0.3 and 0.5. For $x = 0.3$ and 0.5, we observed a gap in the low-temperature CE-type CO phase and a pseudogap with a finite intensity at the E_F in the high-temperature PI

phase. Within the CO phase, the spectral intensity near E_F gradually increased with temperature. These observations are consistent with the results of Monte Carlo simulations on a model including charge ordering and ferromagnetic fluctuations. For $x = 0.25$, on the other hand, little temperature dependence was observed within the low-temperature ferromagnetic insulating (FI) phase and the intensity at E_F remained low in the high-temperature PI phase. We attribute the difference in the temperature dependence near E_F between the CO and FI phases to the different correlation lengths of orbital order between both phases. Furthermore, we observed an upward chemical potential shift with decreasing temperature due to the opening of the gap in the FI and CO phases. The doping dependent chemical potential shift was recovered at low temperatures, corresponding to the disappearance of the doping-dependent change of the modulation wave vector as observed in Chapter 3. Spectral weight transfer with hole concentration was clearly observed at high temperatures but was suppressed at low temperatures. We attribute this observation to the fixed periodicity with hole doping in PCMO at low temperatures.

In Chapter 5, we have experimentally determined chemical potential shift as a function of carrier concentration in NSMO using core-level photoemission spectroscopy. A suppression of chemical potential shift was observed in and around the CE-type CO composition range of NSMO, indicating that there is charge self-organization such as stripe formation or its fluctuations in this range as in the case of PCMO.

In Chapter 6, we have studied chemical potential shift as a function of temperature in NSMO by measurements of core-level photoemission spectra. For ferromagnetic samples ($x = 0.4$ and 0.45), we observed an unusually large upward chemical potential shift with decreasing temperature in the low-temperature region of the FM phase. This can be explained by double-exchange (DE) mechanism if the e_g band is split into non-degenerate bands by dynamical/local Jahn-Teller effect. The shift was suppressed near the Curie temperature (T_C), which we attribute to a crossover from the DE to lattice-polaron regimes. The result was compared with the temperature-dependent chemical potential shifts in other phases of NSMO, namely, those in the CE-type AF CO ($x = 0.5$), A-type AF metallic ($x = 0.55$ and 0.6), and C-type AF insulating phases ($x = 0.7$).

In Chapter 7, we have summarized chemical potential shift as a function of carrier concentration and bandwidth in PCMO, NSMO, and LSMO by measurements of photoemission spectra. Different behaviors of the doping-dependent chemical potential shifts between PCMO, NSMO and LSMO reflect the different strengths of the tendency toward the charge self-organization. With increasing bandwidth, we observed a downward chemical potential

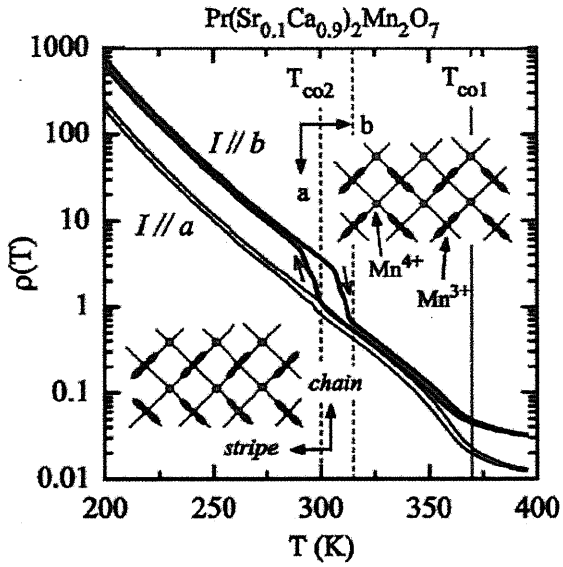

Figure 9.1: Temperature dependences of resistivity in $Pr(Sr_{0.1}Ca_{0.9})_2Mn_2O_7$ for the current direction along the a and b axes [9.15, 16]. Insets represent the charge and orbital ordering in the CO1 and CO2 phases.

shift, probably due to the reduction of the orthorhombic distortion. After subtracting this contribution common to the three systems, we extracted an upward chemical potential shift with increasing bandwidth in the ferromagnetic metallic region $0.3 < x < 0.5$, which we attribute to the enhancement of DE interaction in the Jahn-Teller-split e_g band.

In Chapter 8, we have studied changes in the core-level and valence-band photoemission spectra under ultraviolet-light illumination in PCMO and NSMO. We observed a downward chemical potential shift and enhancement of spectral weight near the E_F when the CE-type CO phase of PCMO was illuminated, which we attribute to a partial melting of the CO phase. We also found a downward chemical potential shift when the FM phase of NSMO was illuminated. We ascibe this to the suppression of the ferromagnetic spin correlation by photogenerated down-spin carriers.

While we have revealed the origins of various complex phenomena in the mixed-valence manganites, many problems remain to be settled in future in order to fully understand the electronic properties of these systems. First, further studies including x-ray scattering and neutron scattering are required for the FI phase of PCMO in order to elucidate the relationship between the suppression of chemical potential shift and the change of the modulation wave vector with hole doping in this composition range. Second,

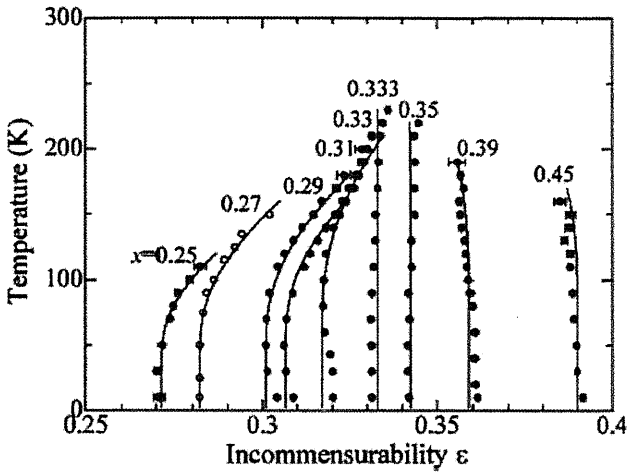

Figure 9.2: Temperature dependences of the incommensurability ϵ of the stripes for $La_{2-x}Sr_xNiO_4$ [9.19].

systematic studies using model Hartree-Fock calculations will be useful to gain further insight into the spin, charge, and orbital ordering in PCMO. Recently, the formation of Zener polarons has been proposed in PCMO with $x = 0.4$ from neutron diffraction data [9.1]. Also, for $x \geq 0.5$, bi-stripe or Wigner-crystal model may be realized for $La_{1-x}Ca_xMnO_3$ and PCMO [9.2, 3]. It is shown by means of model Hartree-Fock calculations that the orbital polarons are stabilized in the PCMO with $x = 0.25$ [9.4]. Thirdly, more detailed measurements of temperature-dependent chemical potential shift in bilayered-system $La_{2-2x}Sr_{1+2x}Mn_2O_7$ using photoemission spectroscopy will provide us valuable information about the applicability and limitation of the DE model. The reported chemical potential shift as a function of temperature for the $La_{2-2x}Sr_{1+2x}Mn_2O_7$ with $x = 0.4$ is opposite to that for the three-dimensional system such as NSMO and LSMO [9.5]. DE model including the dimensionality may provide an important clue for understanding the chemical potential shift with temperature in the $La_{2-2x}Sr_{1+2x}Mn_2O_7$. Fourthly, angle-resolved photoemission spectroscopy (ARPES) studies will be necessary to discuss the band structures and Fermi surfaces of the three-dimensional manganites such as PCMO and NSMO in detail. One can directly determine the k-resolved electronic structure by ARPES measurements. ARPES studies for layered manganites have revealed the importance of electron-phonon coupling for pseudogap or gap formation and the existence of quasiparticle states [9.6, 7, 8, 9]. So far, the difficulty encountered in using ARPES to study the three-dimensional systems has been the

preparation of smooth surfaces at an atomic level because of the lack of a cleavage plane. Recently, high-quality single-crystal thin films grown by the pulse laser deposition have become available for perovskite-type oxides and the band structure of three-dimensional manganites have been investigated using *in situ* ARPES on samples prepared by the pulse laser deposition [9.10, 11, 12, 13, 14]. Fifthly, it will be interesting to investigate the electronic structure of bilayered-system $Pr(Sr_{0.1}Ca_{0.9})_2Mn_2O_7$ using ARPES and core-level photoemission spectroscopy [9.15, 16]. This compound shows a spontaneous rotation of the stripes with temperature. The resistivity curves of $Pr(Sr_{0.1}Ca_{0.9})_2Mn_2O_7$ show two distinct anomalies at $T_{CO1} \sim 370$ K and at $T_{CO2} \sim 300$ K, which is related to the thermally induced rotation of the stripes by 90° as shown in Fig. 9.1 [9.15, 16]. Lastly, the charge self-organization such as stripe formation on a nanometer scale has also been recognized in layered-structure cuprates and nickelates. The suppression of chemical potential shift as a function of carrier concentration has been found in $La_{2-x}Sr_xNiO_4$ and underdoped $La_{2-x}Sr_xCuO_4$ and has been attributed to the incommensurate charge modulation by means of photoemission spectroscopy [9.17, 18]. A commensurate-to-incommensurate crossover with temperature has been observed in the stripes of the $La_{2-x}Sr_xNiO_4$ from synchrotron radiation x-ray diffraction study as shown in Fig. 9.2 [9.19]. More systematic studies of the doping and temperature dependences of chemical potential in these compounds will shed further light on the complex phenomena in strongly correlated electronic systems.

References

[9.1] A. Daoud-Aladine, J. Rodriguez-Carvajal, L. Pinsard-Gaudart, M. T. Fernandez-Diaz, and A. Revcolevschi, Phys. Rev. Lett. **89**, 097205 (2002).

[9.2] S. Mori, C. H. Chen, and S.-W. Cheong, Nature **392**, 473 (1998).

[9.3] P. G. Radaelli, D. E. Cox, L. Capogna, S.-W. Cheong, and M. Marezio, Phys. Rev. B **59**, 14440 (1999).

[9.4] T. Mizokawa, D. I. Khomskii and G. A. Sawazky, Phys. Rev. B **63**, 024403 (2000).

[9.5] K. Schulte, M. A. James, L. H. Tjeng, P. G. Steeneken, G. A. Sawatzky, R. Suryanarayanan, G. Dhalenne, and A. Revcolevschi, Phys. Rev. B **64**, 134428 (2001).

[9.6] D. S. Dessau, T. Saitoh, C.-H. Park, Z.-X. Shen, P. Villella, N. Hamada, Y. Moritomo, and Y. Tokura, Phys. Rev. Lett. **81**, 192 (1998).

[9.7] Y.-D. Chuang, A. D. Gromko, D. S. Dessau, T. Kimura, and Y. Tokura, Science **292**, 1509 (2001).

[9.8] Z. Sun, Y.-D. Chuang, A. V. Fedorov, J. F. Douglas, D. Reznik, F. Weber, N. Aliouane, D. N. Argyriou, H. Zheng, J. F. Mitchell, T. Kimura, A. Revcolevschi, and D. S. Dessau, Phys. Rev. Lett. **97**, 056401 (2006).

[9.9] N. Mannella, W. L. Yang, X. J. Zhou, H. Zheng, J. F. Mitchell, J. Zaanen, T. P. Devereaux, N. Nagaosa, Z. Hussain, and Z. X. Shen, Nature **438**, 474 (2005).

[9.10] M. Shi, M. C. Falub, P. R. Willmott, J. Krempasky, R. Herger, K. Hricovini, and L. Patthey, Phys. Rev. B **70**, 140407(R) (2004).

[9.11] M. C. Falub, M. Shi, P. R. Willmott, J. Krempasky, S. G. Chiuzbaian, K. Hricovini, and L. Patthey, Phys. Rev. B **72**, 054444 (2005).

[9.12] A. Chikamatsu, H. Wadati, H. Kumigashira, M. Oshima, A. Fujimori, N. Hamada, T. Ohnishi, M. Lippmaa, K. Ono, M. Kawasaki, and H. Koinuma, Phys. Rev. B **73**, 195105 (2006).

[9.13] A. Chikamatsu, H. Wadati, H. Kumigashira, M. Oshima, A. Fujimori, M. Lippmaa, K. Ono, M. Kawasaki, and H. Koinuma, Phys. Rev. B **76**, 201103(R) (2007).

[9.14] H. Wadati, A. Maniwa, A. Chikamatsu, I. Ohkubo, H. Kumigashira, M. Oshima, A. Fujimori, M. Lippmaa, M. Kawasaki, and H. Koinuma, Phys. Rev. Lett. in press

[9.15] Y. Tokunaga, T. Lettermoser, Y. Lee, R. Kumai M. Uchida, T. Arima, and Y. Tokura, Nature Materals **5**, 937-941 (2006).

[9.16] Y. S. Lee, Y. Tokunaga, T. Arima, and Y. Tokura, Phys. Rev. B **75**, 174406 (2007).

[9.17] M. Satake, K. Kobayashi, T. Mizokawa, A. Fujimori, T. Tanabe, T. Katsufuji, and Y. Tokura, Phys. Rev. B **61**, 15515 (2000).

[9.18] A. Ino, T. Mizokawa, A. Fujimori, K. Tamasaku, H. Eisaki, S. Uchida, T. Kimura, T. Sasagawa, and K. Kishio, Phys. Rev. Lett. **79**, 2101 (1997).

[9.19] K. Ishizaka, T. Arima, Y. Murakami, R. Kajimoto, H. Yoshizawa, N. Nagaosa, and Y. Tokura, Phys. Rev. Lett. **92**, 196404 (2004).

Acknowledgments

It is my great pleasure to express my special gratitude to the following people for my doctoral thesis.

First of all, I would like to express my deepest gratitude to my supervisor Prof. Atsushi Fujimori for introducing me into the field of condensed matter physics. I would like to thank him for many enlightening discussions, continuous encouragement and his kind guidance throughout this study. I am grateful to Prof. Takashi Mizokawa for a lot of useful advice and enlightening discussions. I have been deeply inspired by his view of physics. I have to express my great thanks to Dr. Teppei Yoshida for giving me a lot of valuable advice.

The experiments at Photon Factory were supported with the members of Oshima Group. I am thankful to Prof. Hiroshi Kumigashira and Prof. Masaharu Oshima for giving me the invaluable opportunity to measure photoemission spectra at Photon Factory Beamline BL-2C. I would like to thank Mr. Akira Chikamatsu for a lot of discussions especially about the research of Mn oxides. Their enthusiastic attitude toward experiments encouraged me during the beam time.

I would like to thank Dr. Yasuhide Tomioka, Prof. Hideki Kuwahara and Prof. Yoshinori Tokura for supplying the excellent samples of $Pr_{1-x}Ca_xMnO_3$, $Nd_{1-x}Sr_xMnO_3$ and $La_{1-x}Sr_xMnO_3$ and informative discussions. The high quality of the samples based on their skilled crystal growth technique provided us with useful and trustworthy data.

Let me thank Prof. Sang-Wook Cheong for providing us with valuable comments on the study of chemical potential shift in $Pr_{1-x}Ca_xMnO_3$. I would like to thank Prof. Pinaki Majumdar for useful advice and enlightening discussions about my recent works.

I am grateful to the members of Fujimori Group. I would like to thank Dr. Hiroki Wadati for teaching me how to perform experiments at Photon Factory Beamline BL-2C and stimulating discussions from many view points. Dr. Jong-Il Hwang instructed me the fundamental principles of photoemission spectroscopy and how to deal with the photoemission spectrometer. Dr. Wadati, Mr. Masaru Takizawa, and Mr. Koji Maekawa have

helped me in the lab experiments. Dr. Hwang, Mr. Yoshitaka Osafune, Mr. Yasuhiro Ooki, Mr. Gyong-Sok Song and Mr. Yuta Sakamoto always collaborated with me in the maintenance of the photoemission spectrometer. I would like to my special thanks to Dr. Yukiaki Ishida for a lot of useful and enlightening discussions about the studies of temperature-dependent chemical potential shift. I would like to thank Dr. Kiyohisa Tanaka, Dr. Hajime Yagi, Mr. Masaki Kobayashi, Mr. Makoto Hashimoto, Mr. Masaki Ikeda, Mr. Satoru Kudo, Mr. Walid Malaeb, Mr. Takashi Kataoka, Mr. Keisuke Ishigami, Mr. Shin-ichiro Ideta, and Prof. Yuanhua Lin for a lot of discussions, advice and warm encouragement. I would also like to thank Ms. Emiko Murayama, Ms. Ayako Fukuya and Ms. Yuko Shimazaki for dealing with a lot of business stuff and giving me encouragement.

I am grateful to the members of Mizokawa Group: Dr. Daisuke Asakura, Dr. Jin-Yong Son, Dr. James Quity, Mr. Kou Takubo, Mr. Thanh Trung Tran, Mr. Shizuka Hirata, Mr. Akira Shibata, Mr. Yasuhiro Fujii, Mr. Yuuki Wakisaka, Mr. Takaaki Sudayama, Mr. Satoru Iwata, Mr. Takashi Iida, Mr. Yousuke Morita, and Mr. Norihisa Takaiwa. They gave me a lot of encouragement and support.

Finally, I wish to thank my family and friends for their various supports.

Tokyo
December 2007

Kazuaki Ebata